國 立 交 通 大 學

機械工程學系

碩士論文

近場光學讀取頭中奈米孔與固態浸沒透鏡整合製程之研究

Study of The Integration Process between The Nano-Aperture and Solid Immersion Lens for Near-Field Recording Pick-Up Head

研 究 生：許鴻隆

指導老師：徐文祥 教授

中華民國九十四年六月

‘

Study of The Integration Process between The Nano-Aperture and Solid Immersion Lens for Near-Field Recording Pick-Up Head

研 究 生：許鴻隆　　Student：Hung-Lung Hsu

指導教授：徐文祥　　Advisor：Wensyang Hsu

國 立 交 通 大 學

機械工程學系

碩 士 論 文

A Thesis
Submitted to Institute of Mechanical Engineer
College of Engineering
National Chiao Tung University
in partial Fulfillment of the Requirements
for the Degree of Master
in

Mechanical Engineering

June 2005

Hsinchu, Taiwan, Republic of China

中華民國九十四年六月

近場光學讀取頭中奈米孔與固態浸沒透鏡整合製程之研究

研究生：許鴻隆　　指導教授：徐文祥

國立交通大學機械工程學系

摘要

在近場光學紀錄系統中，微孔與固態浸沒透鏡（SIL）為常被用來克服光學繞射極以及限縮小光點的兩項技術。其中在微孔系統中，光點大小直接由微孔尺寸所決定，因此我們可藉由縮小微孔尺寸至奈米等級來得到極高解析度，然而由於奈米級微孔之光輸出效率極低，因此在記錄速度上一直無法有效提升。至於利用 SIL，雖然所獲得的光點可較傳統光學記錄系統小，同時仍然可保持高光輸出效率，但其所得到之解析度卻不及微孔所能獲得的。根據以往研究指出，若將微孔與 SIL 結合，則由於入射於微孔的光功率密度增加，因此光出射效率相對得以提升。然而在組裝或黏合奈米孔與 SIL/SSIL 時，必然會產生對準誤差，但如何將奈米孔與 SIL/SSIL 準確結合則至今尚未有文獻討論。本論文之研究重點即是在利用奈/微米機電技術製作 SIL/SSIL 與奈米級微孔之整合結構，其中奈米孔是利用聚焦離子束蝕刻進行製作，而 SIL/SSIL 則是利用熱回流製程進行製作。為了克服對準誤差，本研究提出一種自我對準技術，其方法是利用在熱回流製程中表面張力所自行產生的自我調整機制。在微孔設計方面，論文中也將研究不同形狀之微孔對光輸出效率的影響。在此介紹圓形孔及 C 形孔。

在製作方面，SIL 以及 SSIL 已製作成功，而其最大尺寸誤差皆在 3%以內。在奈米孔方面，已製作出直徑 103nm、148nm、329nm 的圓孔以及尺寸 303nm×205nm、223nm×105nm 的 C 形孔。本研究並藉由掃瞄電子顯微鏡(SEM)證實所提出整合 SIL/SSIL 與奈米孔之自我對準技術的可行性。

在遠場量測結果中，與直徑 329nm 的圓孔比較，SIL 與直徑 329nm 圓孔之整合元件在光輸出率上可增強約 1.68 倍，顯示 SIL 確實有增強奈米孔的光輸出效率，並進一步證實其整合 SIL 與奈米孔結構之自我對準技術的可行性。在 C 形孔量測方面，在保持相同光點大小之情形下，303nm×205nm 的 C 形孔在光輸出效率上比直徑 148nm 圓孔提高 14.325 倍。與直徑 148nm 圓孔比較，直徑 15μm 的 SIL 與 303nm×205nmC 形孔之整合元件在光輸出率方面甚至可增強約 24.438 倍，顯示整合 SIL 與 C 形奈米孔可大幅提昇光學讀取性能。

Study of The Integration Process between The Nano-Aperture and Solid Immersion Lens for Near-Field Recording Pick-Up Head

Student: Hung-Lung Hsu Advisor: Wensyang Hsu

Department of Mechanical Engineering
National Chiao Tung University

Abstract

For near-field recording systems, Aperture and Solid Immersion Lens（SIL） are two popular techniques to overcome light diffraction limit and reduce spot size. In aperture systems, seeing that light spot size is directly determined by aperture size, aperture systems can provide an ultra-high resolution by reducing the aperture size to nano-scale. However, nano-aperture suffers from low power throughput which results in the recording speed unable to be promoted. SIL systems, while can providing a smaller spot size than obtained in conventional optical recording systems with still maintaining high optical throughput, do not have the resolution observed from aperture probe systems. According to previous researches, nano-aperture combined with SIL/SSIL can improve the throughput owing to greater power densities at the aperture. However, the misalignment between the SIL/SSIL and nano-aperture always occurred in assembling or bonding step. How to align the nano-aperture and SIL/SSIL together precisely has not proposed yet. In this research, the purpose is concentrated on combination of SIL/SSIL and nano-aperture by Nano/Micro Electro-Mechanical Systems（N/MEMS） technology, where nano-aperture is fabricated with Focused Ion Beam（FIB）system and SIL /SSIL are formed by thermal reflowing process. In order to overcome the misalignment between SIL/SSIL and nano-aperture, a self-alignment technique based on self-modulation by surface tension during thermal reflowing process is proposed. About aperture designs, the influence of varied shapes of apertures at optical throughput is also studied. Here, circular apertures and C-shaped apertures are introduced.

In fabrication results, SIL and SSIL are fabricated and the maximum error is less than

3% in comparison with the designed values. About nano-aperture, the diameter 103nm, 148nm, and 329nm of circular aperture and the dimensions 303nm×205nm and 223nm×105nm of C-shaped apertures are fabricated. The feasibility of self-alignment technique between SIL/SSIL and nano-aperture proposed in this research is also verified by Scanning Electron microscope（SEM）.

From the measurement results of far-field system, the 15μm-diameter SIL/329nm-diameter circular aperture component has 1.68 times enhancement of throughput compared with 329nm-diameter aperture alone. This result shows that SIL can really enhance the light throughput of nano-aperture and the feasibility of self-alignment technique between SIL and nano-aperture is further verified. About measurement results of C-shaped apertures, the throughput of 303nm×205nm C-shaped aperture alone is 14.325 times larger than that of 148nm-diameter circular aperture alone, while maintaining a comparable near-field spot size. Even the throughput of 303nm×205nm C-shaped aperture/15μm-diameter SIL component can be enhanced by 24.438 times as compared with 148nm-diameter circular aperture alone. This result indicates that combination of SIL and C-shaped aperture can really greatly enhance the performance of near-field pick-up head.

誌謝

在交大這即忙碌又充實的兩年真的讓我學習及成長許多，包括在半導體製程、微機電設計及光儲存上的研究..等。在歷經了兩年的努力終於完成了這本碩士論文，首先謝謝我的指導教授：徐文祥老師能給我這個機會並帶領我學習微機電這領域，同時提供我們在實驗上無匱乏的儀器、材料及經費，讓我們能無後顧之憂的完成實驗。

在實驗的執行上，特別感謝林郁欣學長給我這個機會，成為國科會精密儀器發展中心的研究生，以使用聚焦離子束機台(FIB)。在操作期間感謝鄭紹章學長在機台(FIB)上的指導與信任，讓我得以親自進行操作並順利完成奈米孔之製作。同時感謝交大光電所的方仁宇學長、陳予潔同學在專業知識、量測設備上的提供與協助，讓我能順利完成實驗。

再來當然還要感謝實驗室的學長：楊涵評學長、鍾君煒學長、張俊偉學長、黃家聖學長、張育儒學長、梁志豪學長、戴文川學長在製程經驗上的傳授與援助。感謝兩位美麗的學姐：邱雅惠學姐、蔡梨暖學姐、同學：佳曄、毅家、業達、學弟：昌旗、元德、彥宏的陪伴與關心。

最後，由衷的感謝我最愛的家人：明星爸爸、傅霞媽媽、文星叔叔、金幼阿姨、淑雯姊姊、鴻濱哥哥、女友瓊文在背後一直默默的支持我、關心我，當我心情低落或實驗不順利時能夠給我最溫馨的鼓勵，同時忍受我的壞脾氣，是我能完成學業的最大動力。我想我要感謝的人、要感謝的話真的的太多了，不是三言兩語所能道盡的，在此，僅以這本論文獻給關心我及我關心的人，謝謝你們，謝謝。

鴻隆 謹于 新竹交通大學

June 2005

Contents

List of Figures

List of Tables

Chapter 1 Introduction

1.1 Motivation

The technology of optical data storage has grown up greatly. Fig. 1.1（林盈熙, 1999）shows the roadmap of the storage density. From CD to single-layer DVD, the data capacity has grown about 7.2 times. Furthermore, in blu-ray, since the wavelength of light is down to 405nm, the data capacity can be promoted to 25GB per layer on a 120-mm diameter disk. In conventional optical storage systems, including red-ray system or blu-ray system, data storages are read or written in far field. Owing to light diffraction limit in far-field, light cannot be focused to an arbitrarily small spot even by a perfect lens free from aberrations. According to near-field recording theorem, the spot size is not restricted by diffraction limit if the data storage system is operated in near-field. There are many devices were proposed to reduce the spot size for near-field recording. However, how to fabricate a pick-up head for near-field optical data storage with high light throughput has become an important issue.

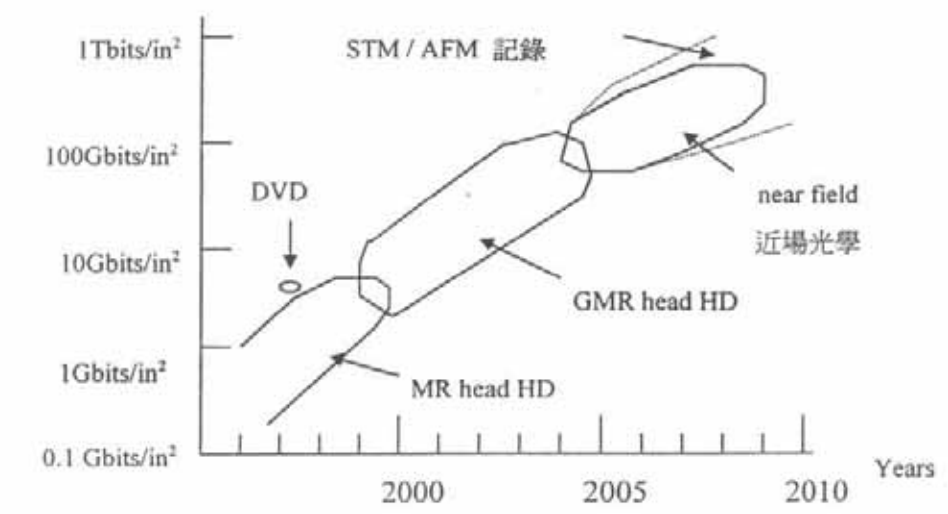

Fig. 1.1 The roadmap of data storage density（林盈熙, 1999）.

1.2 Conventional recording

In conventional recording, the spot diameter only focused by an objective lens in far field can be expressed as:

D_{spot} λ/N.A.....1-1

N.A. = n*sinθ……..……1-2

λ is the wavelength of incident light and N.A. is the numerical aperture of objective lens. n is the refractive index which is equal to 1 within the air environment. From Eq. 1-1, it can be found that smaller λ or using an objective lens with high N.A. can shrink spot size and then increase data capacity. Fig. 1.2 shows that the light source focused on the media surface by the objective lens reads or writes data, where the disk is so-called substrate-incident disc.

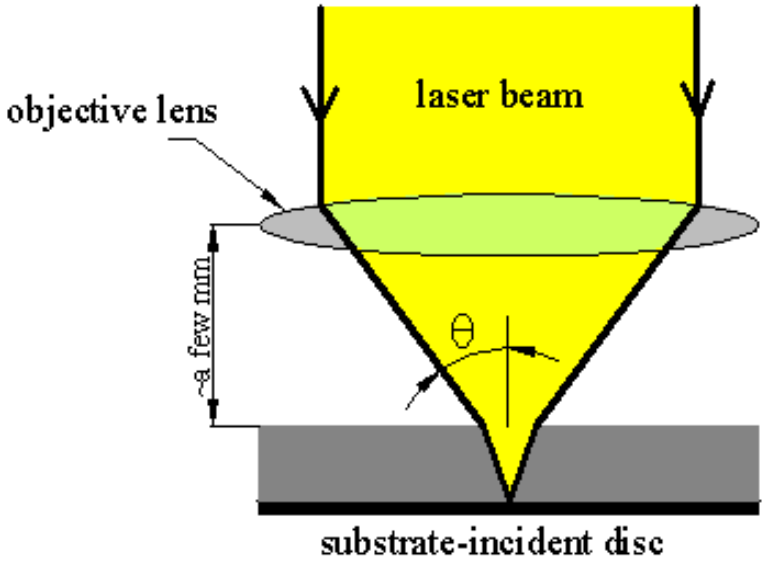

Fig. 1.2 Schematic diagram of conventional recording.

1.3 Principle of Near-Field optics

In conventional optical recording, the spot size is restricted to light diffraction limit. For near-field optical data storage, two major components, Solid immersion lens（SIL） and sub-micro aperture have been proposal in order to overcome the light diffraction limit. In the following sections, the related principles of near-field optics are described.

1.3.1 Near-Field recording with solid immersion lens

In 1994, the research group in Stanford University proposed a new design for optical data storage to reduce the spot size efficiently [Kino et al. 1994]. The different point from conventional optical recording is added a so-called solid immersion lens（SIL） between the objective lens and disk. As shown in Fig. 1.3, seeing that the refractive index of SIL (n_1) is larger than 1, the speed of the incident laser beam within the SIL is slowed down. In other words, the light wavelength within the SIL becomes λ/n_1 so the final spot size focused on the bottom surface of SIL by objective lens can be shrunk by a factor of n_1 in comparison with the structure without SIL. When the incident angle θ_1 of light is larger than the critical angle θ_c, the focused laser light on SIL/air interface suffers total internal reflection and creates transmission light wave, so called evanescent wave. Without the evanescent wave, the well-defined spot focused by objective lens only exists in SIL. According to electro-magnetic wave theorem, the distribution of transmission electrical field E_T can be expressed as:

$$\vec{E}_T = \vec{E}_2 e^{-\alpha z} e^{j\beta y} \quad \text{1-3}$$

$$\alpha = k_2 \sqrt{\frac{n_1^2}{n_2^1}\sin^2\theta_1 - 1} = k_2 \sqrt{n_1^2 \sin^2\theta_1 - 1} \quad \text{1-4}$$

$$\beta = k_2\left(\frac{n_1}{n_2}\sin\theta_1\right) = k_2\left(n_1\sin\theta_1\right) \quad \text{.....1-5}$$

Where n_2 is refractive index of air which is equal to 1, θ_1 is the angle of incident light which is larger than θ_c, k_2 is the wave vector in the air environment and α is defined as the skin depth which approximates λ. From Eq. 1-3, it is found that the transmission light wave or called evanescent wave only exists within a distance which is smaller than the wavelength of incident light because it decays exponentially. Therefore, the gap size between the SIL and the disc must be precisely controlled and the conventional substrate-incident disk must be replaced with the surface-incident disk.

Fig. 1.4 shows another configuration of SIL lens, so called superhemispherical SIL (SSIL). The distance between the bottom surface of SSIL and the center of curved surface is r/n_1., where r is radius of SSIL. The SSIL bends the light at the curved surface and focuses the incident light on the SSIL/air interface. Since not only the wavelength within the SSIL is shortened by a factor of n_1, but the $\sin\theta$ is also increased by a factor of n_1, the spot diameter can be reduced by a factor of n_1^2 according to Eq.1-1.

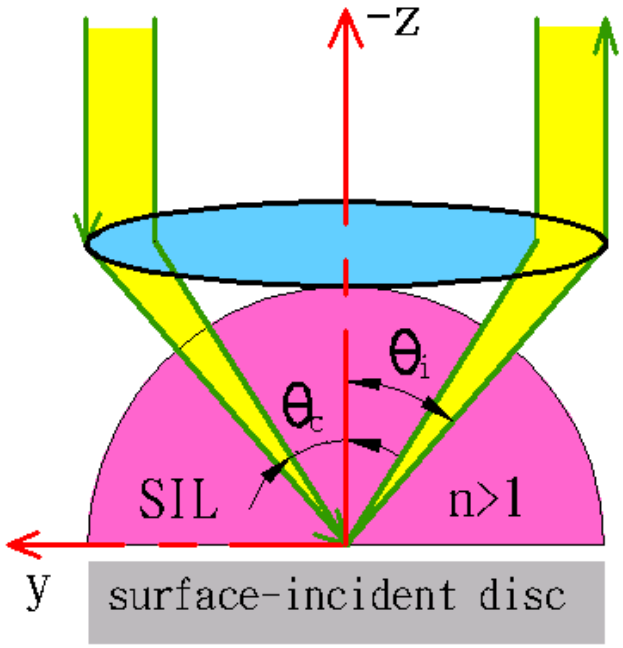

Fig. 1.3 Optical data storage structure with solid immersion lens.

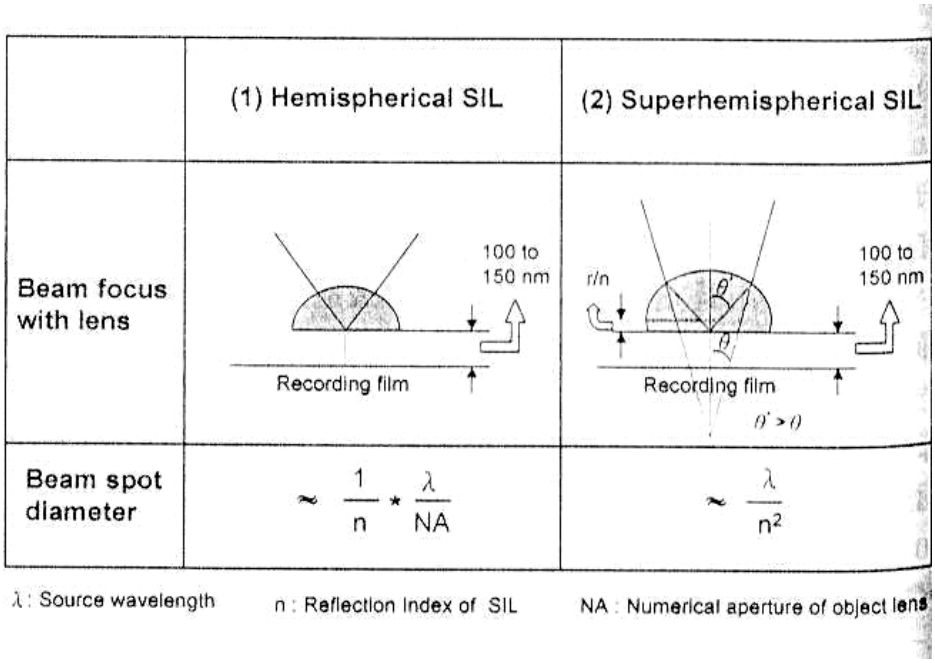

Fig. 1.4 Principles of SIL and SSIL（蔡定平，1998）.

1.3.2 Near-Field recording with sub-micro aperture

If there is an diameter ***a*** of aperture, at z =0 the light intensity can be expressed as：

$$I(r, z=0) = \exp(-\frac{r^2}{a^2}) \quad \text{.....1-6}$$

By using fourier transform of Eq.2-6, a gaussian distribution of transverse wave vector (k_r) can be found and the relation of k, k_r, and k_z can be expressed as follows:

$$k^2 = k_r^2 + k_z^2 \quad \text{.....1-7}$$

Where k is wave vector at vacuum which is equal to $2\pi/\lambda$, k_r is the component of k in x direction and k_z is the component of k in z direction. λ is the wavelength of the incident light.

If k_r<k, k_z is a real number and the wave is a propagating wave. On the contrary, if the k_r>k, k_z is an imaginary number and the wave is an evanescent wave.

If a better resolution wants to be obtained, the k_r must be larger than 1/a. Here, it is assumed that ***a*** must be smaller than λ and then the analysis can be further expressed as follows:

$$\begin{aligned} &a << \lambda \text{ and } k^2 = k_r^2 + k_z^2 \\ &k_r >> k \Rightarrow -k_r^2 \approx k_z^2 \\ &k_z \approx ik_r \approx i/a \end{aligned} \qquad \text{.....1-8}$$

From Eq.2-8, it is found that when a<<λ, k_z is an imaginary number. The light wave is an evanescent wave and the length of attenuation is about a distance of a. For this reason, if we want to overcome the light diffraction limit with using sub-micro aperture, two requirements should be met:

1. The aperture diameter must be smaller than light wavelength.
2. The distance between the disc and aperture must be smaller than light wavelength.

1.4 Related Research

Many research groups have proposed various novel methods to overcome the diffraction limit. SIL and sub-micro aperture are the key components to realize near-field recording. The fabrication methods of SIL/SSIL, sub-micro aperture, combination with SIL and aperture, and integrated pick-up head will be discussed in the following sections.

1.4.1 Fabrication of SIL/SSIL

In 2000, Yee et al. reported a micro-molding method to fabricate SSIL. As shown in Fig. 1.5, hemispherical dome-shaped pits are isotropically etched in a single crystalline silicon substrate. After putting into an optical grade PMMA powder in the silicon master, the mold is heated above the glass transition temperature of PMMA. By a proper pressurizing, cooling, and releasing processes, the uniform micro solid immersion lens can be produced.

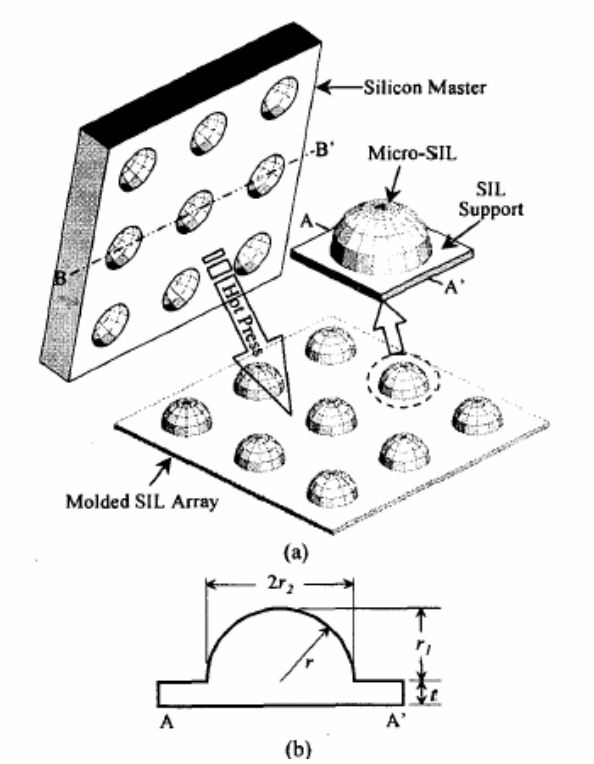

Fig. 1.5 Fabrication of the SIL by press molding (Yee et al., 2000).

In 2001, Lin et al. reported a new method to fabricate micro-ball lens in a planar substrate. As Fig. 1.6 indicates, the process concept is that at first, polyimide is spin coated on the substrate and a thick photoresist(AZ4620) is then patterned on the polyimide film. During development, the exposed PR and the polyimide can be etched at the same time. The final process is heat treatment at 190℃ for 12hr. Because the glass transition temperature of AZ4620 is smaller than 190℃, it begins to become the liquid-like photoresist and tends to reduce the surface energy. By controlling the pattern dimensions of AZ4620, the different sizes of micro-ball lens can be formed.

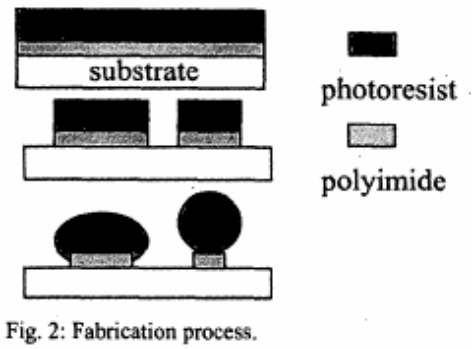

Fig. 2: Fabrication process.

Fig. 1.6 Fabrication process of microlens array (Lin et al., 2001).

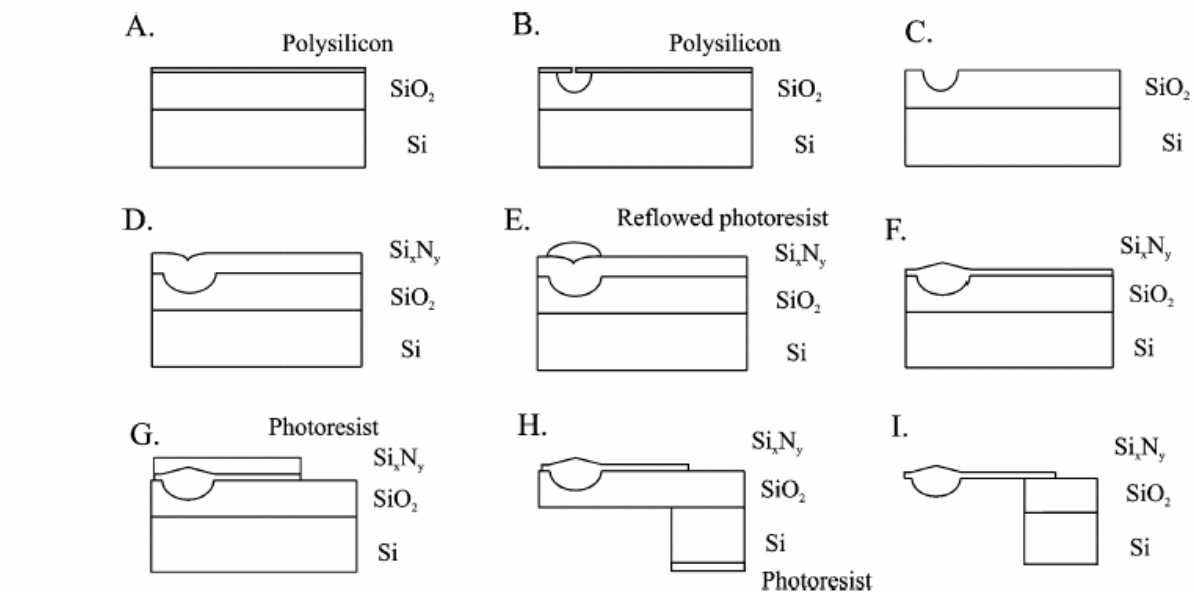

Fig. 1.7 Fabrication process for silicon nitride SILs (Crozier et al., 2002)

In 2002, Crozier et al. proposed micromachined method to fabricate silicon nitride solid immersion lens. The fabrication process is shown in Fig. 1.7. By deposition and etching process, the dome-shape fillister is isotropically etching in the silicon dioxide layer. After depositing silicon nitride, the PR is patterned on silicon nitride film and reflowed thermally. Plasma etching is then used to transfer the PR into the underlying silicon nitride layer to form a tip. It is noticeable that the plasma etch recipes must be controlled to give approximately equal etch rates for the silicon nitride and PR. Finally, by plasma etching backside Si wafer and wet etching silicon nitride film, the SILs integrated with cantilever beams can be formed.

1.4.2 Fabrication of sub-micro aperture

In 1998, Pilevar et al. introduced a focused ion-beam (FIB) fabrication method to produce a tiny aperture. As Fig. 1.8 indicates, the ion beam is raster scanned within the rectangle region to precisely remove the tip of glass fiber coated with a 100-150 nm aluminum. Typically, the diameter of the opening aperture is smaller than 100 nm.

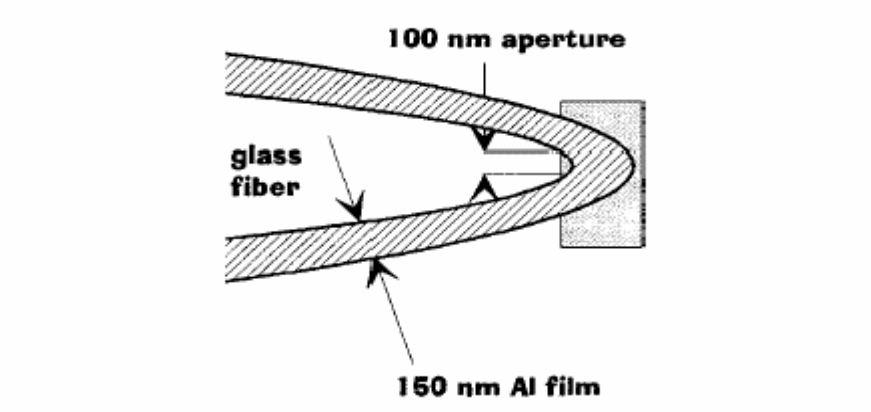

Fig. 1.8 Using FIB milling procedure to produce a near-field aperture (Pilevar et al, 1998)

In 1999, Phan et al. represented a novel fabrication process to batch produce the tiny apertures. The fabrication process is shown in Fig. 1.9. First, the gap for capacitance detection, side of cantilever and etch pit for the tip are formed by oxidation, lithography, silicon dioxide patterning and Si etching step. Then, a thick thermal oxide film is grown at 1050℃. Due to the effect of locally compressive intrinsic stress with the oxide, the thermal oxide film at the bottom of a pyramidal etch pit is thinner. After the partly etching with BHF solution, the aperture at tip of pyramidal is formed.

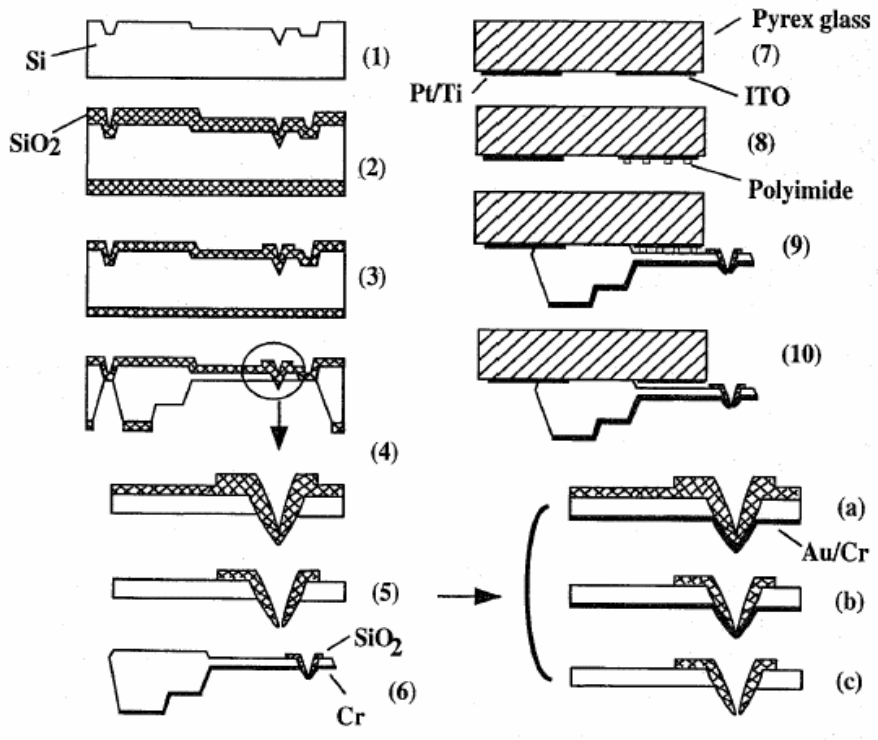

Fig. 1.9 Fabrication of a fiber tip by chemical etching (Phan et al. 1999).

In 2000, Suzuki et al. introduced a so-called solid-solid diffusion method to fabricate the near-field aperture. Fig. 1.10 indicates that the probe is coated with chalcogenide film such as Te by sputtering and then a metal such as Ag is contact with Te. Since Ag can diffuse into Te coated on the probe, the alloy is produced at the contact area after several hours. The alloy is only left on Ag film after removing the cantilever from the Ag film because the mechanical strength of Te is weaker than that of Ag. The aperture size can be adjusted by controlling the contact area, temperature, and time.

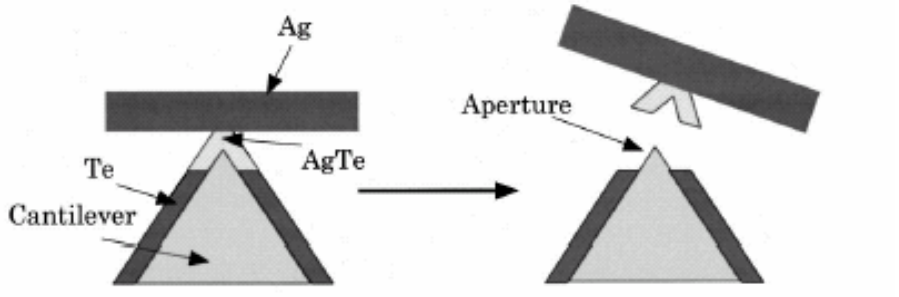

Fig. 1.10 Schematic diagram of solid-solid diffusion method（Suzuki et al., 2000）.

In 2001, Lane et al. proposed a low cost method to fabricate sub-micro aperture. As shown in Fig. 1.11, an array of initial aperture size is defined by lithography process and then overelectroplating method is adopted to shrink the initial-aperture. The electroplating parameters controlling the diameter of final aperture include electroplating time and current density etc.

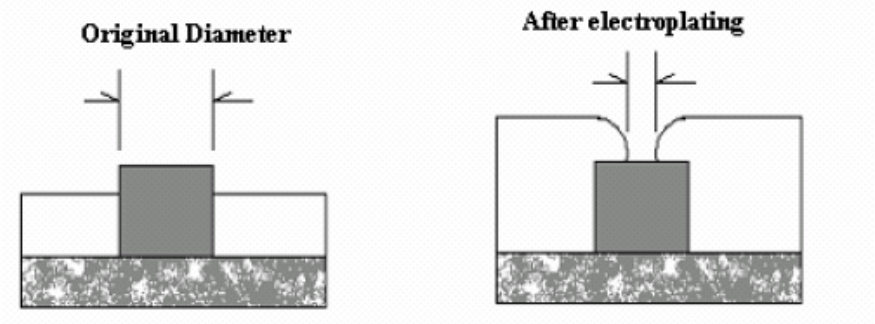

Fig. 1.11 Schematic diagram of making a sub-micro aperture by over-electroplating (Lane, 2001).

1.4.3 Combination with SIL and aperture

Solid immersion lens systems and aperture probes are two popular methods to reduce spot size. However, for conventional square apertures, the power throughput from the aperture decays as the fourth power of aperture size when the aperture size is much smaller than the light wavelength. The resolution observed from solid immersion lens system is not as good as that observed from aperture probes. In 2001, Milster et al. represented a new method based on the combination of a SIL and an aperture probe to overcome the shortcoming of the techniques used separately. Fig. 1.12 illustrates the fabrication process. At first, a 2 μm thick SiN membrane is fabricated. A 100nm thick Al is deposited on the membrane next. An array of 200nm×350nm apertures is then cut with FIB. Finally, SIL is attached to the backside of SiN membrane. Because the light source is focused and the spot size illuminating the aperture is shrunk by SIL compared with the spot size with fiber-based or far field illumination, the light throughput can be greatly improved. The resolution is mainly determined by the aperture size. However, the SIL and aperture is not easy to align precisely in assembly process.

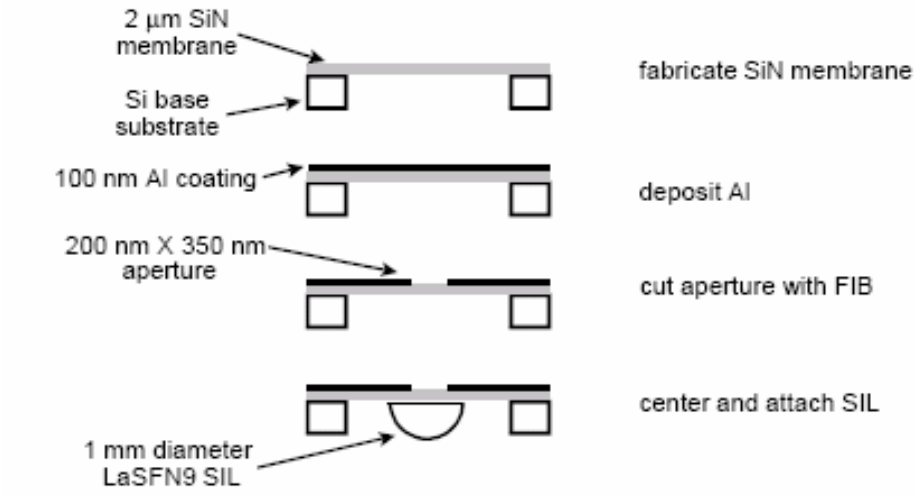

Fig. 1.12 Fabrication process for aperture array combined with SIL (Tom D. Milster et al., 2001).

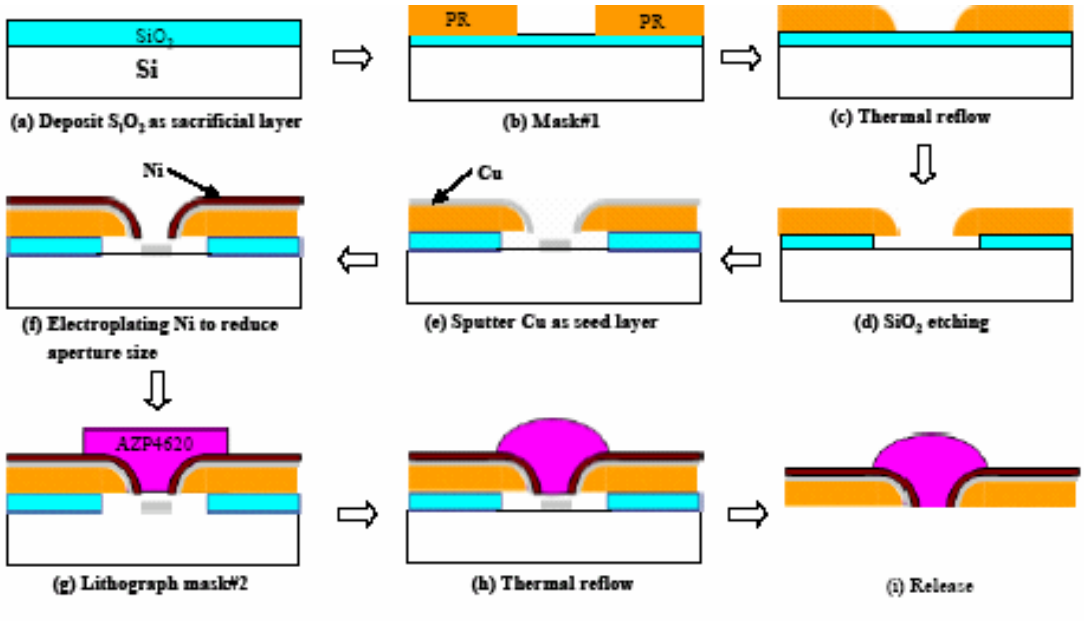

Fig. 1.13 Fabrication process of the sub-micro aperture combined with microlens (Chou et al., 2002).

In 2002, Chou et al. proposed another method to combine sub-micro aperture and SIL. The fabrication process is shown in Fig. 1.13. The photoresist (AZ4620) is patterned by lithography and then thermal reflowed to form a slope sidewall which can allow more light illuminating the aperture. After electroplating, the initial aperture can be shrunk to a sub-micron size. Finally, SIL is formed on the aperture by patterning a photoresist and then reflowing thermally. However, the misalignment between aperture and SIL is still existent.

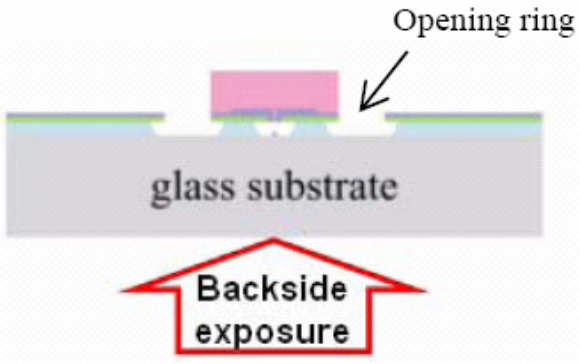

Fig. 1.14 The self-alignment mechanism between SIL and aperture (Chang et al., 2004).

In 2004, Chang et al. proposed a self-alignment process between SIL and aperture for near-field recording pick-up head. As shown in Fig. 1.14, the initial aperture and pedestal is first made by lift-off process and then the opening ring is formed by wet etching. The aperture and opening ring is concentric owing to the same lithography process. By backside exposure, the pattern of photoresist (AZ4620) can be precisely aligned with the aperture. Finally, the SIL is formed by reflowing thermally. The initial aperture is shrunk by sputtering and evaporating metal but this shrinkage step is failed owing to the bad step coverage of physical vapor deposition (PVD). The laser spot size through the aperture of NFR pick-up head with and without SIL is 2.1 μm and 3.0 μm. It is clear that the SIL has 30 % shrinkage efficiency.

1.4.4 Integrated Pick-Up Head

For the application of optical storage technology, individual component, like optical fiber, SIL/SSIL, and aperture, are integrated together to form a pick-up head.

In 2000, Kato et al. proposed a structure for near-field recording. This device combined SIL and aperture component is shown in Fig. 1.15. The incident light guided by fiberlens and focused by planar microlens is transmitted into the aperture. In this case, individual parts were fabricated separately, so that every part must be aligned and bonded precisely.

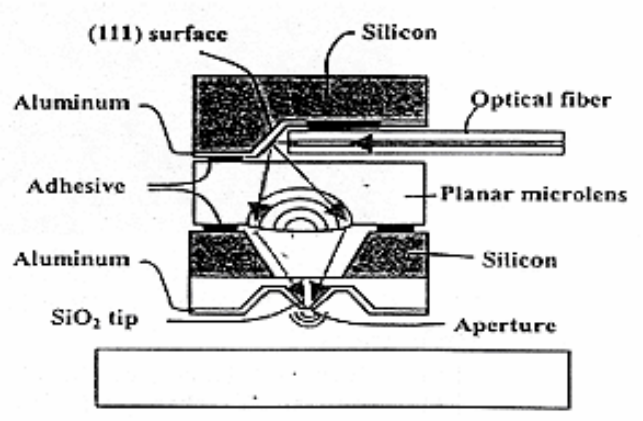

Fig. 1.15 Cross section of the near-field optical pick-up head（Kato et al. , 2000）.

The MO recording is one of the most popular recording systems. When the medium is heated by a laser spot to the Curie point (~200℃), the orientation of the magnetic domain which is very resistant to change at room temperature can be determined by extra magnetic field. The magnetization direction of the domain is fixed after cooling down. The recorded marks can be detected by the polarization rotation due to the Kerr effect. In the following paragraphs, the related researches of the MO structure combined with SIL and sub-micro aperture are depicted.

In 1998, TeraStor Corporation proposed the MO pick-up head combined with SIL and microcoil. As shown in Fig. 1.16, the laser beam is focused on the bottom surface of SIL lens by the objective lens and then creates evanescent coupling. The gap size between the SIL and the disc can be precisely kept about $\lambda/3$ to $\lambda/4$ with the air bearing slider. The main advantage with this device is that the data can be directly overwritten by heating the local spot with evanescent coupling and adding extra magnetic field with microcoil, simultaneously.

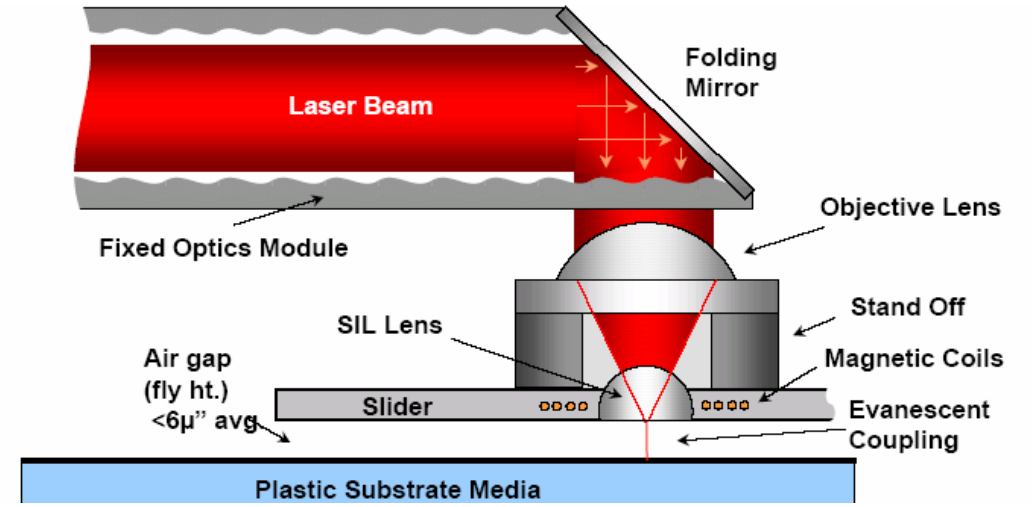

Fig. 1.16 The MO pick-up head combined with the SIL and microcoil (Terastor, 1998).

In 2003, Shieh et al. proposed a new structure on MO pick-up head by MEMS technology. As Fig. 1.17 indicates, the device is composed of the air bearing slider, a V-groove with a 45° mirror, hemispherical-shaped fiberlens, the SSIL, and an aperture. The laser beam is guided by the fiber and then reflected by the 45° mirror into the SSIL. The light transmission through the aperture can be greatly enhanced, because the light spot illuminating the aperture is shrunk by SSIL. This work was supported by the Ministry of Education of the Republic of China for promoting academic excellence of universities in "Photonic Science and Technology for Tera Era". Finishing the integration structure is one of my current purposes.

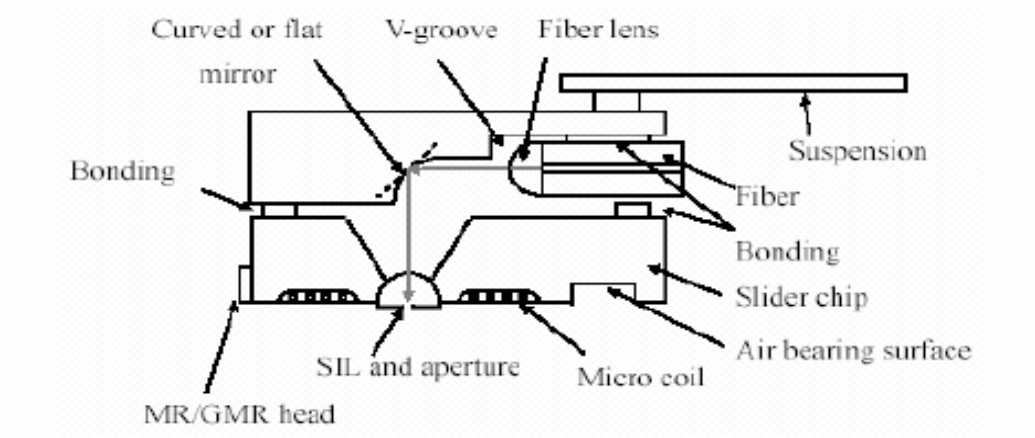

Fig. 1.17 Near-field optical pick-up head structure (Shieh et al., 2003).

1.5 Current approach

For near-field optical data storage, Solid Immersion Lens systems and Aperture probes are two popular methods to reduce spot size. The fabrication methods of sub-micro aperture, including FIB patterning, electroplating, wet etching and solid-solid diffusion method were presented. Then, the SIL/SSIL formation methods include thermal reflowing, micro-molding and micromachined method. In aperture systems, seeing that light spot size is directly determined by aperture size, aperture systems can provide an ultra-high resolution by reducing the aperture size to nano-scale. However, nano-aperture suffers from low power

throughput which results in the recording speed unable to be promoted. SIL systems, while can providing a smaller spot size than obtained in conventional optical recording systems with still maintaining high optical throughput, do not have the resolution observed from aperture probe systems. According to previous researches, nano-aperture combined with SIL/SSIL can improve the throughput owing to greater power densities at the aperture. Hence, how to overcome the misalignment between SIL/SSIL and aperture becomes a primary mission to develop this integrated system. If the misalignment which is inevitable in assembling or bonding step is occurred, the light passing through the SIL/SSIL will not focus on the nano-aperture. In 2004, Chang et al. proposed a self-alignment technique based on backside exposure to overcome this problem. However, the diameter of aperture is about 2 μm.

Here, this research is concentrated on fabricating the combination of SIL/SSIL and nano-aperture by MEMS technique without bonding or assembly and measure the light throughput enhancement effect of SIL/aperture component in comparison with aperture alone. The nano-aperture as definition of spot size is patterned with Focused Ion Beam system (FIB). The SIL/SSIL as the component to focus and reduce the spot size illuminating the aperture is fabricated by reflowing thermally. In order to overcome the misalignment problem, a self-alignment process based on self-modulation by surface tension during thermal reflowing process is proposed to align SIL/SSIL and nano-aperture together for the near-field pick-up head. About aperture designs, varied shapes of apertures are also studied to whether affect the optical throughput or not, where the different dimensions of nano-aperture containing circular and C-shaped apertures are fabricated and then compared.

Chapter 2 Design

2.1Concept design

As shown in Fig. 2.1, it is known that combining SIL/SSIL and aperture together can provide smaller spot size with good throughput.

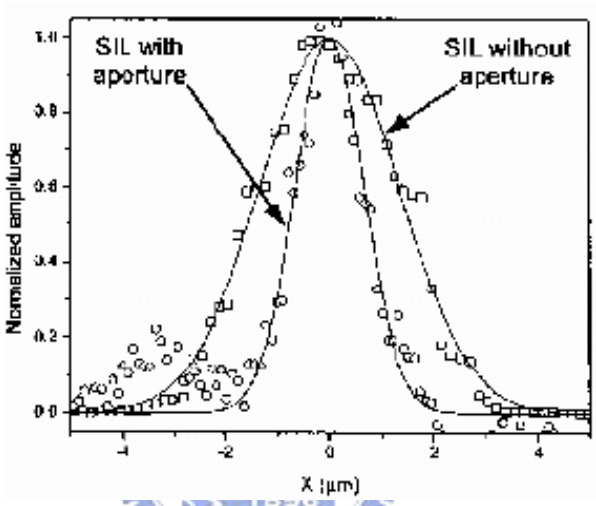

Fig. 2.1 Intensity distribution of the laser beam with and without the sub-micro aperture (Fletcher et al., 2000).

A schematic diagram of the proposed near-field pickup head is shown in Fig. 2.2. Light source is guided into the optical fiber and then collimated and shaped by the front-end fiber-lens. The light beam is then reflected by a 45 degree mirror and transmitted into the SIL/SSIL. Because the refractive index（n）of SIL/SSIL is larger than 1, the spot size focused by the SIL/SSIL and illuminating the nano-aperture is reduced by a factor of n for SIL or n^2 for SSIL, which can increase the light throughput in comparison with using an aperture alone. The final spot size is determined by nano-aperture. In this research, the purpose is concentrated on combination of SIL/SSIL and aperture, as shown in the broken line of Fig. 2.2, and measure the light throughput enhancement effect of SIL/aperture component

in comparison with aperture alone. In addition, varied aperture shape will also be designed to study the light throughput enhancement effect.

After describing the main object in this research, the mechanism of self-alignment process and the concept design of individual parts for pickup head are depicted in the following sections.

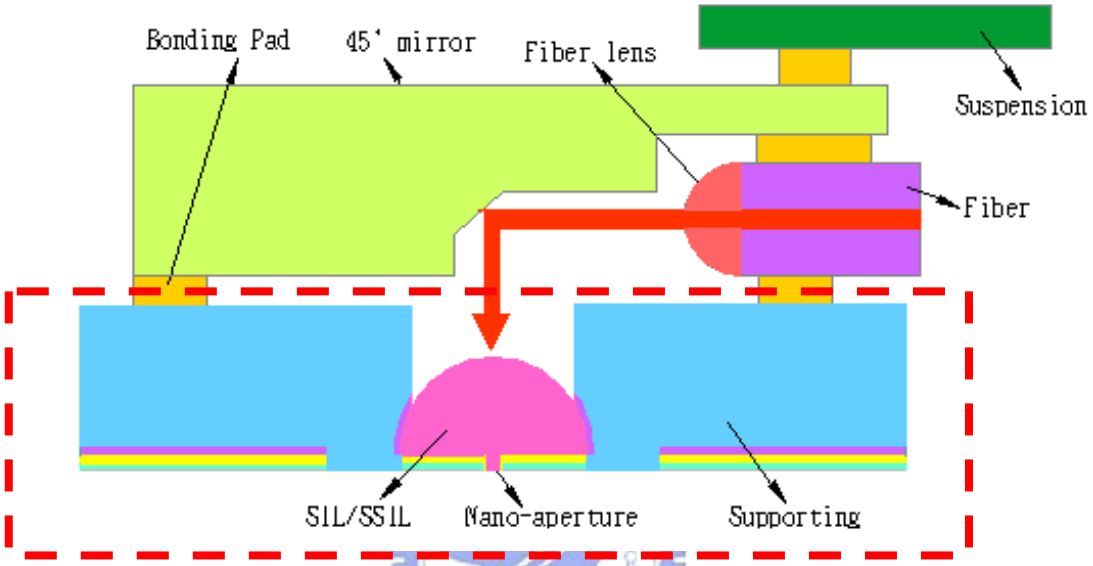

Fig. 2.2 Integrated near-field pick-up head structure.

2.2 Self-alignment design

Near-field pick-up head combined with SIL/SSIL and nano-aperture can provide a smaller spot size with good throughput. Therefore, how to align precisely between SIL/SSIL and nano-aperture becomes a key component. If there is a misalignment, the light passing through the SIL/SSIL will not be focused on the nano-aperture which may cause the device to fail. For this reason, beside the self-alignment process of ***"Backside Exposure Method"*** proposed by Chang in 2004 between SIL and aperture, here a new self-alignment process called "***Surface Tension Modulation Method***" between SIL/SSIL and aperture on glass substrate is investigated.

2.2.1 Surface Tension Modulation Method

This process can be used to form SIL/SSIL combined with nano-aperture without any misalignment. The mechanism is shown as Fig.2.3. At first, the nano-aperture and opening ring are first patterned with Focused Ion Beam（FIB）in the same step so they are concentric. Next, by using chemical solution, the sacrificial layer in the opening ring region is undercut until the glass is exposed. After the coated photoresist is UV exposed with mask#3 （Fig. 2.3（a））, backside exposure is then performed（Fig. 2.3（b））. Because UV light could pass through the opening ring in backside exposure step after Al etching, the columnar photoresist can be defined after development by adjusting the dose quantity of backside exposure which is just enough to expose the photoresist in opening ring region, as shown in Fig. 2.3（c）. Finally, the patterned photoresist is heated over its glass transition temperature, at which the liquid-like photoresist will tend to reduce itself surface energy and become a circular shape. By a suitable heat treatment time, the SSIL may be formed, with the result as illustrated in Fig. 2.3（d）. Even though a little misalignment between the pedestal and the columnar photoresist is occurred in columnar photoresist defining step, as shown in Fig. 2.3（a）, the surface tension at photoresist/pedestal interface may drag the liquid-like photoresist to right position and correct the final shape of SSIL during heat treatment. Therefore, the misalignment can be overcome.

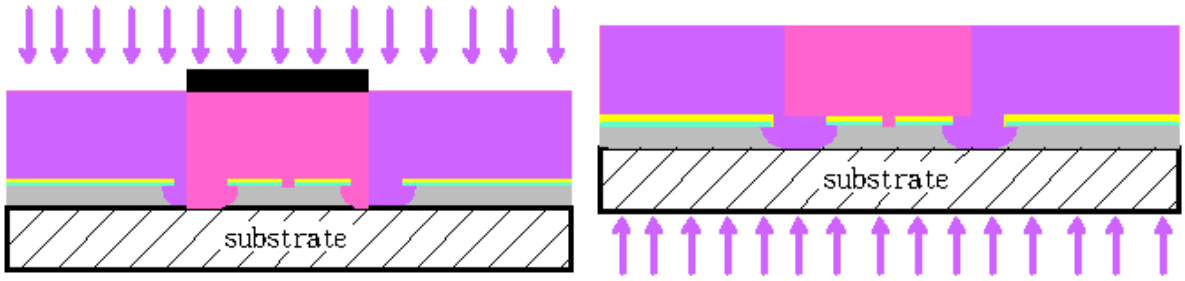

（a） （b）

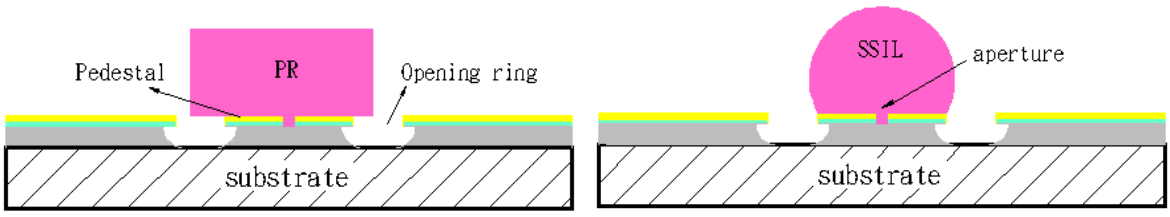

(c) (d)

Fig. 2.3 The self-alignment mechanism of surface tension modulation method.

2.2.2 Backside exposure method

Here, the self-alignment process of backside exposure method is also used to align nano-aperture and SIL. This mechanism is similar to the process of surface tension modulation method. The major difference is the dose quantity of backside exposure. Besides, backside exposure method performs self-alignment in backside exposure step, whereas surface tension modulation method performs that in thermal reflowing step.

Following undercutting the sacrificial layer in opening ring region, the coated photoresist is exposed with mask#1 (Fig. 2.4 (a)) and backside exposed (Fig. 2.4 (b)) with using pedestal as mask in turn. The columnar photoresist being self-alignment with the nano-aperture and opening ring can be defined by adjusting the dose quantity of UV exposure which is much larger than that of surface tension modulation method, as shown in Fig. 2.4(c). After reflowing thermally, the nano-aperture and SIL can be integrated without misalignment, with the result as illustrated in Fig. 2.4 (d).

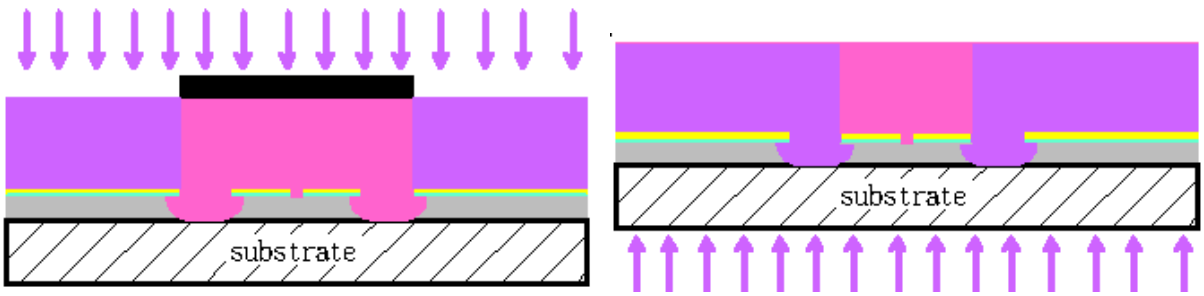

(a) (b)

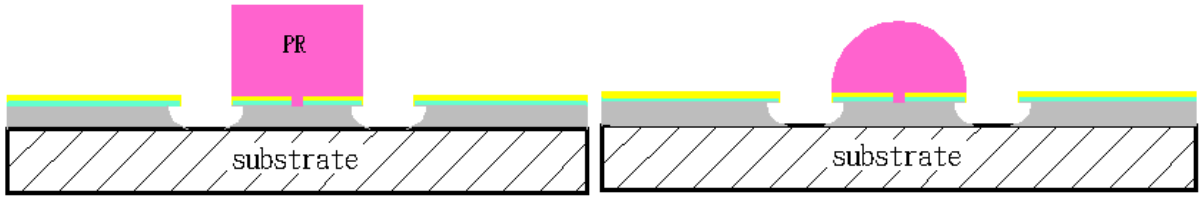

(c) (d)

Fig. 2.4 The self-alignment mechanism of backside exposure method.

2.3 Design of individual parts

The dimensions and materials of the key components in near-field pick-up head will be discussed in this section. The different sizes of the devices will be designed.

2.3.1 The nano-aperture

Focused Ion Beam system（FIB） is generally used as nano-patterning or machining. The applications of FIB include：

- Cross-sectional imaging through semiconductor devices (or any layered structure)
- Modification of the electrical routing on semiconductor devices
- Failure analysis
- Preparation for physico-chemical analysis
- Preparation of specimens for transmission electron microscopy (TEM)
- Micro-machining
- Mask repair
- Non-semiconductor applications

The introduction of FIB and the design of nano-aperture are described as followed.

2.3.1.1 Introduction of Focused Ion Beam system（FIB）

One type of near-field data storage system utilizes a planar metallic nano-aperture to directly define the minimum spot size. Here, the Focused Ion Beam（FIB） is used to pattern the nano or sub-micro aperture. FIB system usually uses a Gallium as the ion source which

can be operated at low beam currents for imaging or high beam currents for site specific sputtering or milling. If FIB is used as microscope, the low current ion beam rasters over the surface of a sample in a similar way as the electron beam in scanning electron microscope （SEM）. The generated secondary electrons (or ions) are collected to form an image of the surface of the sample. If FIB is used as patterning, the high current ion beam is accelerating concentrated to a specific site to cut away or mill any exposed material in the sample, such as hole or surface. By introducing gases or an organic gas compound, FIB can selectively etch one material much faster than surrounding materials, or deposit a metal or oxide. Fig. 2.5 shows the schematic structure of FIB system.

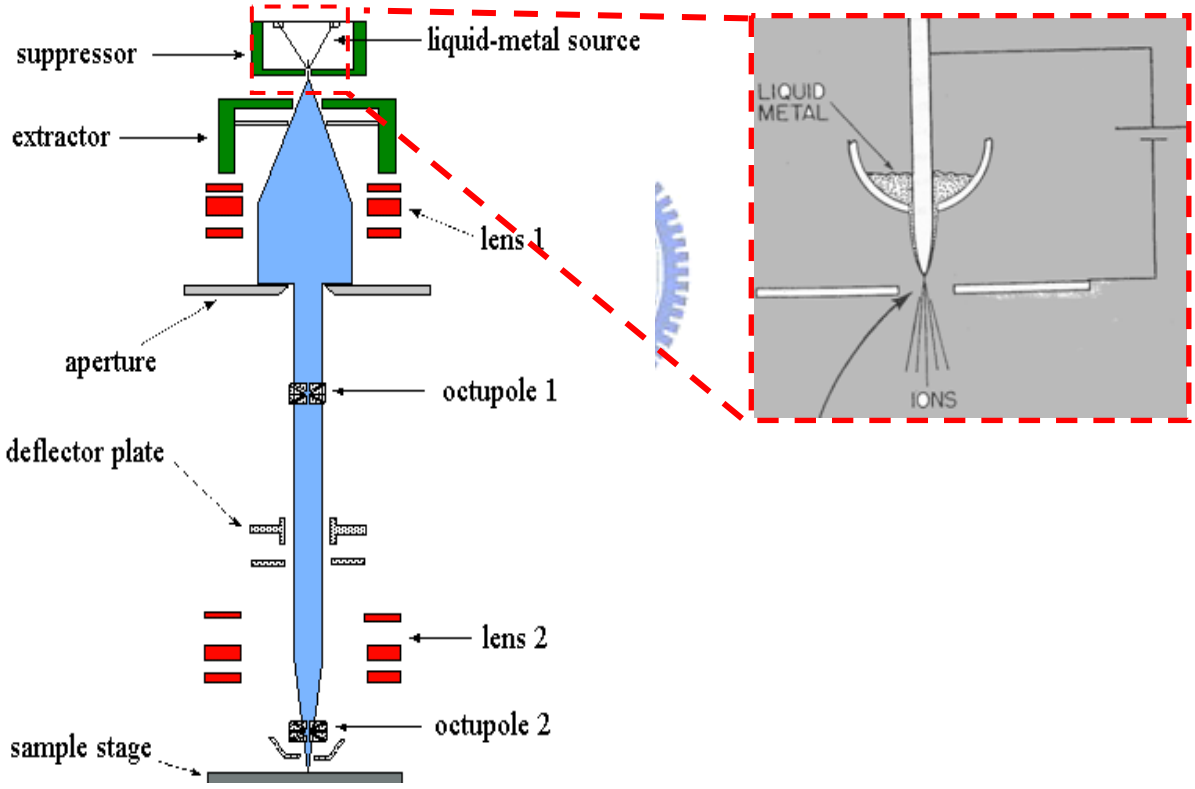

Fig. 2.5 The schematic illustration of Focused Ion Beam system（IBM Almaden Research Center）.

2.3.1.2 Design of the nano-aperture

Fig. 2.6 shows a plot of the aperture design. At first, Ti film as adhesion layer and gold film as pedestal layer are deposited by sputtering. Nano-aperture and opening ring are

then patterned with focused ion beam (FIB) simultaneously so that they are a concentric circle structure. It deserves to be mentioned that the ion beam with a smaller ion current can pattern the smaller dimensions of aperture, whereas the fabrication time is increased with a smaller ion current. After FIB patterning, the lateral wall of aperture forms a slope sidewall which can improve light throughput owning to a larger aperture size on the top surface of Au pedestal layer. The precise diameter of aperture D is defined on the bottom surface of Ti layer. The total thickness T also depends on the dimensions of the aperture. The aperture sizes can not be defined too small when the total thickness is too thick. For this reason, T is designed as 220nm to ensure that D can be patterned to designate diameter.

Theoretically, by reducing the aperture size, the near-field spot size can be made as small as required. Unfortunately, a rapid decrease in the throughput of the aperture is observed with D<60 nm owing to D nearly equal to cutoff diameter of HE11 mode which is about 30nm. Here, the diameter 100nm, 150nm and 350nm of apertures designed will be fabricated with FIB, respectively.

Circular aperture has been shown to exhibit exponential decay in their transmission with increasing film thickness. According to some researches, a C-shaped aperture can overcome the large attenuation due to cross-sectional area and exhibit waveguiding properties, overcoming the exponential decay with film thickness. Therefore, in addition to circular aperture, C-shaped aperture is also interested to study. Fig. 2.7 shows the parameters of C-shaped aperture. Here, the two difference dimensions of C-shaped apertures which are simulated and designed by Fang in 2005, as shown in Fig. 2.8, will also be patterned with FIB system.

In following measurement equipment setup, the light source is set to focus on the top of nano-aperture, which can improve light throughput because the light spot size illuminating the aperture is reduced by a factor of n with SIL or n^2 with SSIL. The parameters of aperture designed are listed in Tab. 2.1.

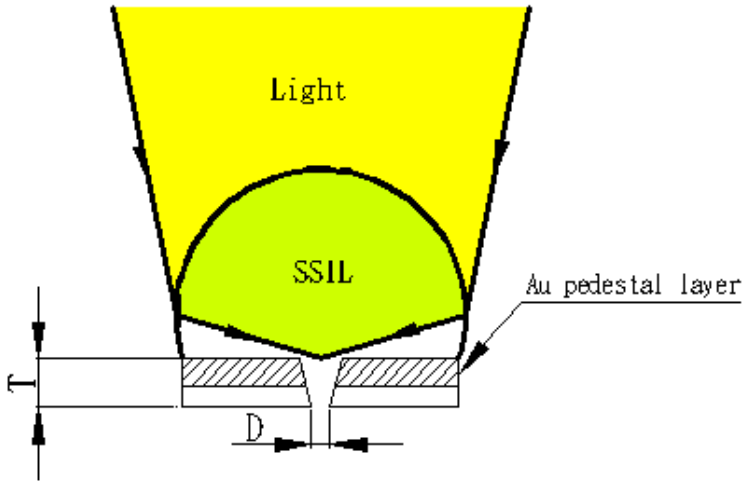

Fig. 2.6 The schematic illustration of the aperture design.

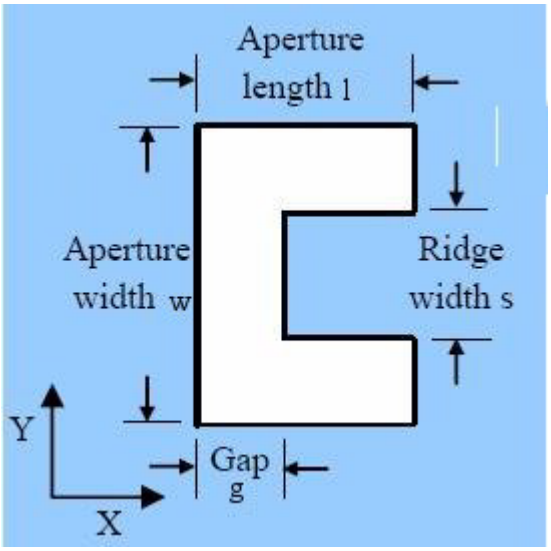

Fig. 2.7 The parameters of C-shaped aperture.

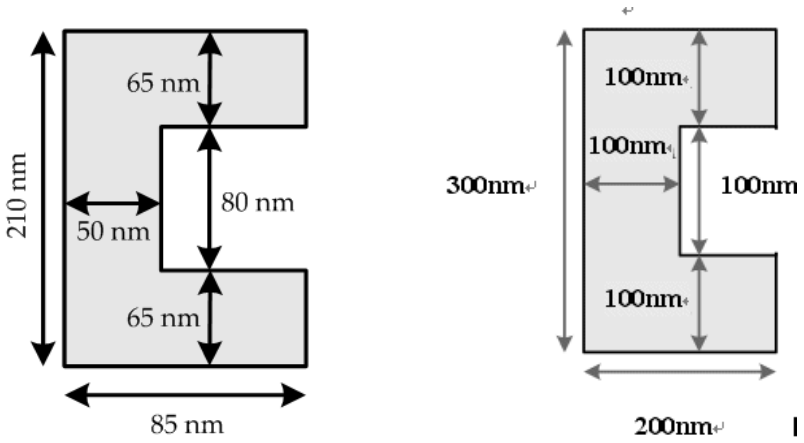

（a）Dimensions #1　　（b）Dimensions#2

Fig. 2.8 The geometrical dimensions of the designed C-shaped apertures.

Tab. 2.1 The design dimensions of aperture.

Aperture shape	D	The thickness of Au	The thickness of Cr	T
Circle	150、350 nm	200 nm	20 nm	220 nm
C-shape	Dimensions#1、2			

2.3.2 SIL/SSIL Design

The geometry of standard SIL and SSIL structure is shown in Fig. 2.9 . In this section, the basic theory of thermal reflowing and the concept design of SIL/SSIL are described.

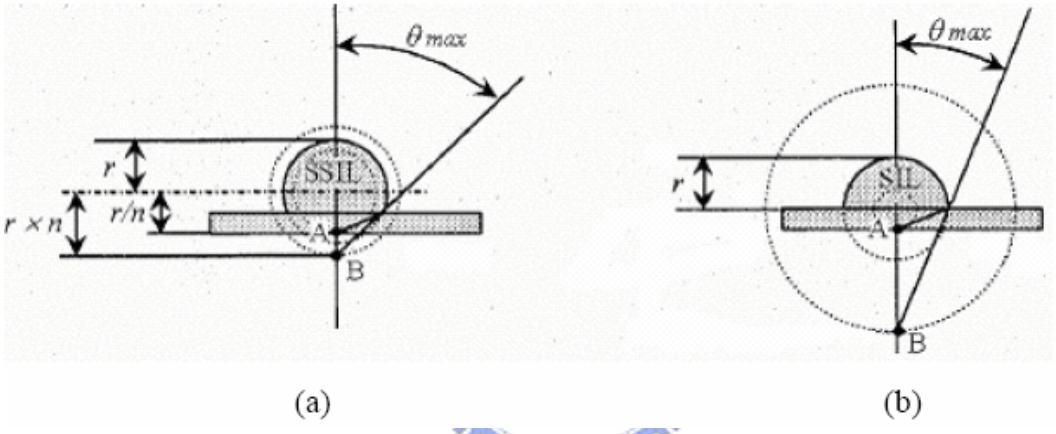

Fig. 2.9 Geometry of (a) SSIL and (b) SIL structure.

2.3.2.1 Basic Theory of Thermal Reflowing

As shown in Fig. 2.10. If the columnar photoresist is heated over its glass transition temperature, it becomes liquid-like. The contact angle changes with the variation of surface energy until stable state. In accordance with the static equilibrium, the function of a liquid drop can be written as the following equation：

$\gamma_{LS} = \gamma_{AL}\cos\theta$ and $\gamma_{SA} = \gamma_{AL}\sin\theta$ （after thermal reflow）……2-1

Where θ is the equilibrium contact angle, γ_{AL} is the surface tension of the liquid, γ_{SA} is the surface energy of the solid and γ_{LS} is the solid/liquid interface energy.

Because the liquid-like photoresist tends to equilibrate the surface tension (Eq. 2-1) and reduces its surface energy during the thermal reflowing process, it becomes a circle-like

structure and change its shape until the minimum surface energy. By controlling D and T, the ideal sizes of SIL/SSIL can be formed.

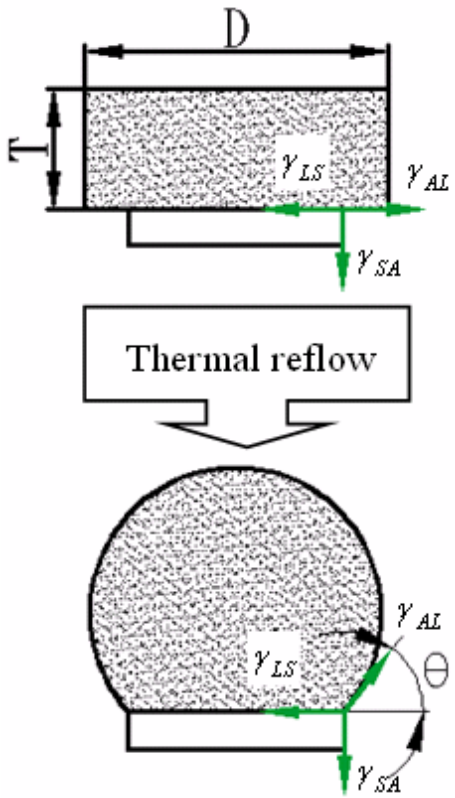

Fig. 2.10 Schematic diagram of the thermal reflow process.

2.3.2.2 The SSIL design

Here, photoresist AZ-4620 is chosen as the material of SIL/SSIL. The design parameters of SSIL are shown in Fig. 2.11. Before reflowing, the volume of columnar photoresist can be expressed as：

$$V_{cylinder} = \pi\left(\frac{C'}{2}\right)^2 \times t \quad \text{.....2-2}$$

After reflowing, the volume of SSIL can be calculated by volume integration and then it can be expressed as：

$$V_{SSIL} = \frac{1}{12}\pi d^3 + \int_0^b \int_0^{2\pi} \int_0^{\sqrt{(a^2 - z^2)}} r dr d\theta$$

$$= \frac{1}{12}\pi d^3 + \left(\frac{\pi d^2}{4} \times z - \frac{\pi z^3}{3} \right)_0^b$$

$$= \frac{1}{12}\pi d^3 + \left(\frac{\pi d^2}{4} \times b - \frac{\pi b^3}{3} \right) \quad \text{.....2-3}$$

For ideal SSIL, the distance between the bottom surface of SSIL and the center of the curved surface can be written as：

$$b = \frac{d}{2n} \quad \text{.....2-4}$$

Where n is refractive index of SSIL. Then, according to Pythagoras' Theorem and Eq.2-4, the diameter of SSIL can be further derived as：

$$d = \sqrt{\left(\frac{C^2 n^2}{n^2 - 1} \right)} \quad \text{.....2-5}$$

It is assumed that the volume of photoresist doesn't change during the thermal reflowing process. Thus, according to Eq. 2-2 ~ 2-5, the thickness of columnar photoresist can be derived, and that is：

$$t = \frac{C^3}{6C'^2} \left(\frac{2n^3 + 3n^2 - 1}{\sqrt[2/3]{(n^2 - 1)}} \right) \quad \text{.....2-6}$$

Actually, the volume of photoresist shrinks during thermal reflowing. Therefore, a parameter of shrinkage ratio ***S*** must be added to Eq.2-6. The modified thickness of columnar photoresist can be expressed as：

$$t_{SSIL} = \frac{C^3}{6C'^2} \left(\frac{2n^3 + 3n^2 - 1}{\sqrt[2/3]{(n^2 - 1)}} \right) \Big/ (1 - S) \quad \text{.....2-7}$$

S is about 0.2~0.4.

It is noticeable that refractive index is different from varied incident light wavelength. The refractive index for AZ-4620 film measured by spectroscopic ellipsometry at light

wavelength 633nm is plotted as Fig. 2.12 as a function of the reflowing time with reflowing at 190℃. It is clear that the refractive index is increased with adding the reflowing time while it almost does not change with the reflowing time over 6 hr. Here, the reflowing temperature and reflowing time is selected to be 190℃ and 12hr, respectively. The refractive index is about 1.74 under this condition.

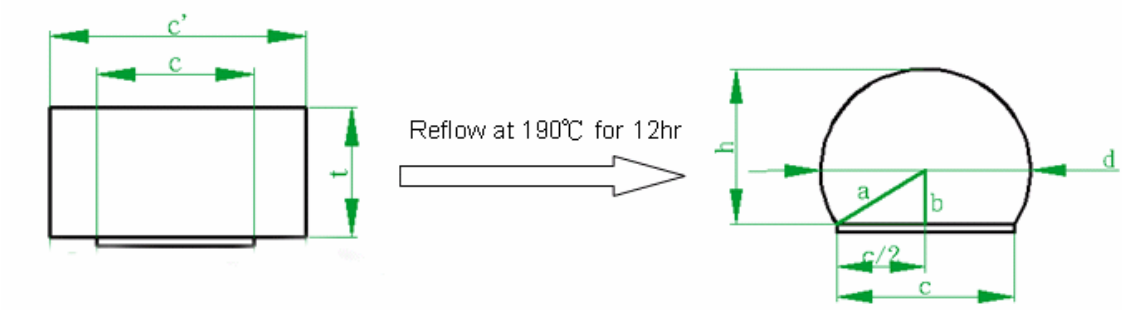

Fig. 2.11 The schematic diagram of the design parameters of SSIL.

`

C：The diameter of pedestal

C′：The diameter of columnar photoresist

t：The thickness of columnar photoreist

d：The diameter of SSIL

a：The radius of SSIL

b：The distance between the bottom surface of SSIL and the center of the curved surface

h：The height of the lens after thermal reflowing

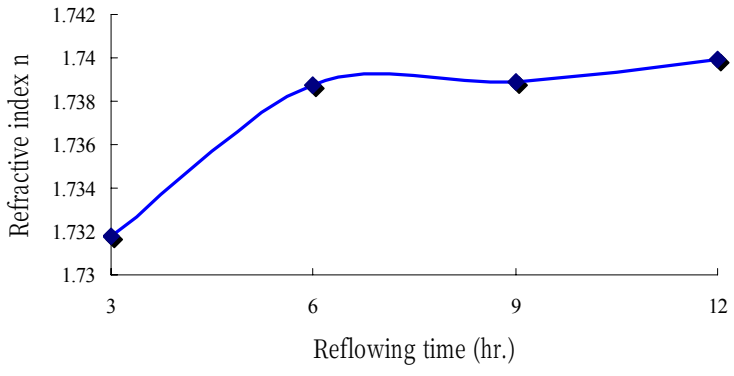

Fig. 2.12 The refractive index for AZ-4620 film at light wavelength 633nm versus the reflowing time with reflowing at 190℃.

2.3.2.3 The SIL design

For SIL, the volume can be defined as:

$$V_{SIL} = \frac{1}{12}\pi d^3 \quad \text{.....2-8}$$

From Eq.2-2 and 2-8, , the thickness of columnar photoresist can be derived, and that is：

$$t = \frac{1}{3}\frac{d^3}{C'^2} \quad \text{.....2-9}$$

Seeing that the photoresist will shrink after reflowing thermally, a parameter of shrinkage ratio ***S*** is also added to Eq.2-9. The modified thickness of columnar photoresist can be expressed as：

$$t_{SIL} = \frac{1}{3}\frac{d^3}{C'^2}\Big/(1-S) \quad \text{.....2-10}$$

For the near-field pick-up head combined with SIL/SSIL and aperture in this research, there are several issues that should be taken into considerations:

1. The nano-aperture and opening ring is patterned with FIB system. The ion beam with a smaller ion current can pattern an aperture with smaller dimensions as well as an opening ring, simultaneously but the total fabrication time will increase, even that the FIB system might not permit to pattern due to too small ion current. In order to define a nano-aperture and a well-suited dimension of opening ring at the same time, the diameter of pedestal is designed to 15 μm.
2. Considering misalignment between the pedestal and the columnar photoresist, the diameter of columnar photoresist is larger than that of pedestal by 10 μm.

3. The minimum thickness of photoresist AZ-4620 chosen as the material of SIL/SSIL is about 5 μm. The integrated structure combined with nano-aperture and 15 μm-diameter SIL can not be fabricated by using surface tension modulation method as the self-alignment technique under issue1 and 2 because ideal thickness of columnar photoresist is about 3 μm, in other words, 5 μm-thickness is too thick. In order to integrating a nano-aperture and a 15 μm-diameter SIL, the self-alignment process of backside exposure method will supersede surface tension modulation method.

Fig. 2.13 shows the light source absorption versus thickness of AZ-4620. I_o means the output intensity of light and I_f means the input intensity of light. In accordance with the above designs and issues, the design parameters of SIL and SSIL are listed in Tab. 2.2.

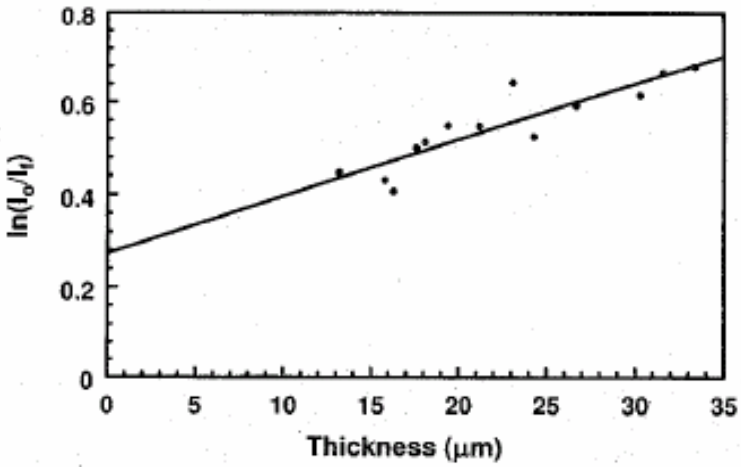

Fig. 2.13 Light source absorption versus thickness of AZ-4620 (King et al., 1996).

Tab. 2.2 The design parameters of SIL/SSIL.

	C	C'	t'	d	b	h	T.E.(%)
For SIL	15	15	7.8	15	—	7.5	69.7
For SSIL	15	25	9.4	18.3	5.3	14.45	64

（T.E.= Transmission Efficiency)

Chapter 3 Fabrication

3.1 Fabrication process combined with SIL/SSIL and nano-aperture.

The general fabrication flowchart of near-field pick-up with the self-alignment techniques is shown in Fig. 3.1.

(a)

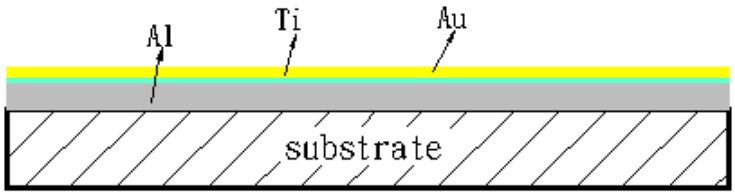

The Al, Ti, and Au film is deposited on the silicon substrate, respectively.

(b)

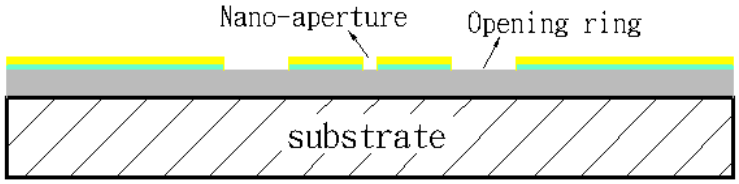

The nano-aperture and opening ring is patterned with FIB.

(c)

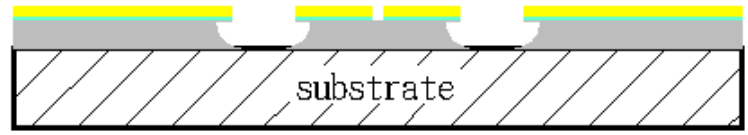

The sacrificial layer Al is etched by Al etchant.

(d) (e)

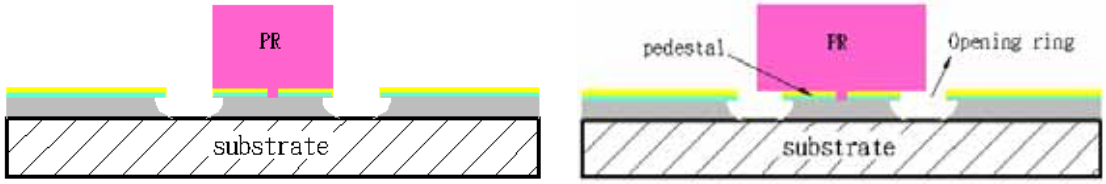

The AZ-4620 is patterned by mask and backside exposure.

(f)

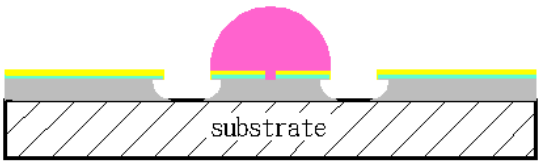

(g)

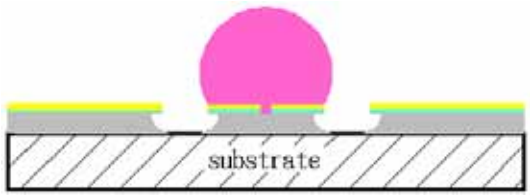

The PR is reflowed thermally.

(h)

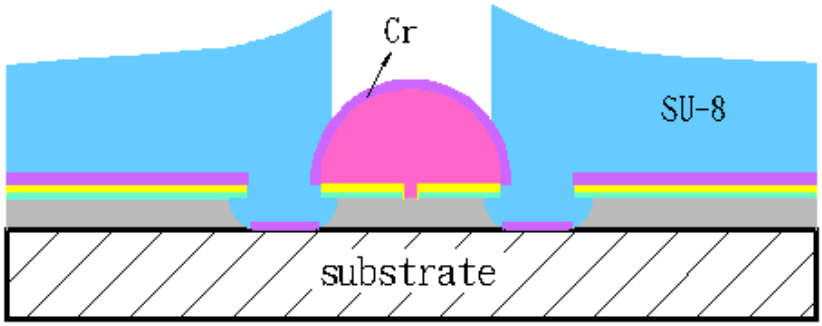

After depositing Cr layer, the SU-8 is patterned by mask#2.

(i)

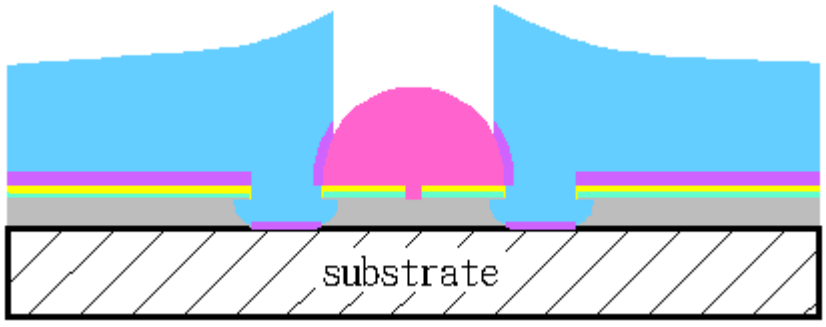

Opening the Cr layer on the SIL by CR-7T.

(j)

Etching sacrificial layer Al for releasing.

Fig. 3.1 The general fabrication flowchart of near-field pick-up head.

3.2 Process of the nano-aperture

As shown in Fig. 3.1（a）, 4-in glass wafers is applied to RCA clean. Next, Al film 1.5um as sacrificial layer is deposited by thermal evaporating on glass wafer. Ti films 20nm as adhesion layer and Au 200nm as pedestal layer are then deposited by sputtering. After metal deposition, the 4-in wafer is sawed to 15mm×15mm square dices by dicing saw system. In next step, nano-aperture and opening ring are patterned on the 15mm×15mm square dice with FEI NOVA 200 FIB tool which is a dual beam system（Scanning electron microscope & Focused ion beam）, with the result as illustrated in Fig. 3.1（b）. The illustration of FIB system is shown in Fig. 3.2. It is noticeable that the ideal etching depth of aperture and opening ring is controlled to just stop on the Al film, nevertheless, over-etching is needed to ensue completely removing the Au/Ti films. Because aperture and opening ring is patterned in the same step, they are a concentric circle structure. Following FIB patterning, Al etchant（80%H_3PO_4+5%HNO_3+ 5%CH_3COOH+10%H_2O）is used to undercut the Al layer until the glass in the opening ring is exposed（Fig. 3.1（c））. The next step is to fabricate SIL/SSIL.

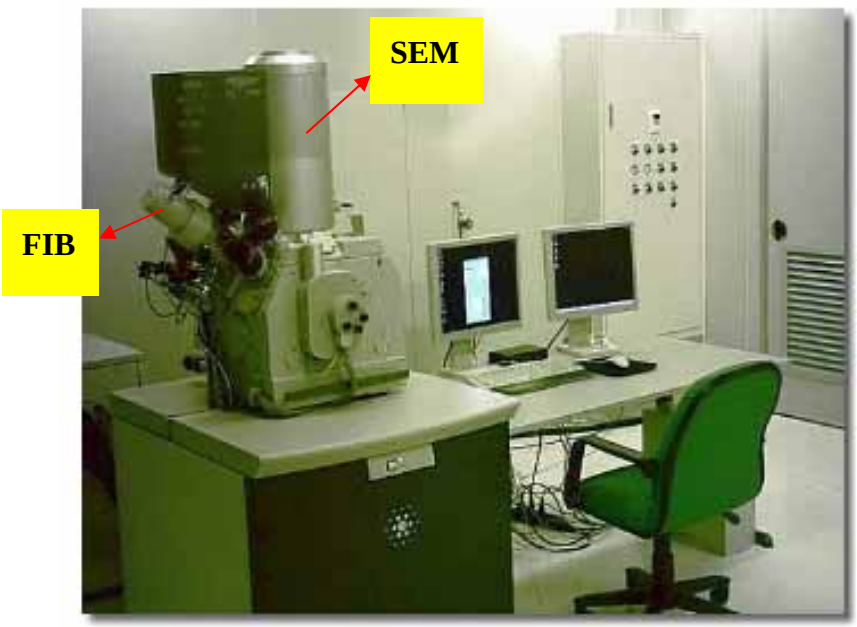

Fig. 3.2 The photograph of FEI NOVA 200 FIB tool.

3.3 SIL formation and self-alignment process

In order to fabricate SIL/SSIL easily, positive photoresist AZ-4620 is chosen as the material of SIL/SSIL. After undercutting Al film, SIL is formed to integrate with the nano-aperture, which can improve the light throughput with good resolution. At first, photoresist (AZ-4620) 7 μm is spin-coated and patterned with mask#1 and backside exposure with using Au pedestal layer as the mask is performed next. The parameters of photolithography are listed in Tab.3.2. Seeing that UV light can pass through the glass wafer and opening ring, the photoresist around the opening ring will be exposed. After development, only photoresist on the pedestal layer will be remained, as shown in Fig. 3.1（d）. Because the columnar photoresist and pedestal are concentric, the SIL and aperture can be combined without misalignment after reflowing thermally at 190℃ for 12hr（Fig. 3.1（f））. Following SIL formation, Cr cover layer is deposited by physical sputtering. The Cr film has two functions, one is protect solvent from permeating into the SIL during SU-8 coating and softbake, and the other is protect the SU-8 development from etching SIL during development. Then negative photoresist SU-8 as a support and connection between SIL and other part of pick-up head is patterned with mask#2（Fig. 3.1（h））. In order to make light source can pass through the SIL, the Cr film is etched with SU-8 as mask, with the result as illustrated in Fig. 3.1（i）. Finally, the Al sacrificial layer is released by KOH（Fig. 3.1（j））.

Tab. 3.1 Basic parameters of coating AZ-4620 7 μm.

Process step	parameters	equipment
photoresist	AZ-4620	—
spin coating	1st Spin: 500 rpm for 10 sec 2nd Spin: 1600rpm for 40sec	JAPAN KYOWARIKEN K-359SD-1
Soft bake time	Baking at 90°C for 90 sec	Hotplate
Exposure time	12 sec	JAPAN K-310P-100S
Development time	120-130 sec 【FHD-5】	—

It should be noted that after coating thick photoresist, the edge of die will remain thicker photoresist film, called "edge bead" effect. If the edge bead is not removed, it will cause incomplete contact between the photomask and the photoresist, and errors occurred in transferring the patterns from mask to photoresist due to light diffraction. Therefore, in order to get the best resolution using contact lithography, it is a necessary step to remove the "edge bead". A common method eliminating "edge bead" effect is using Acetone to removing the edge photoresist film on the 15mm×15mm square dice before UV exposure.

3.4 SSIL formation and self-alignment process

The self-alignment process of ***"Backside Exposure Method"*** is not suited to fabricate SSIL combined with aperture. It is only suited to form the integrated structure of SIL and aperture owing to the light diffraction effect during backside exposure step. After development, there is some pattern loss of the columnar photoresist which make the diameter of photoresist has a gap with the boundary of pedestal. Therefore, even though the patterned photoresist is thick enough, the standard SSIL might not be easy to form. This reason might be that the surface tension around the boundary of columnar photoresist does not form SSIL easily under a pattern loss.

Here, a self-alignment process called "***Surface Tension Modulation Method***" is proposed to avoid the misalignment between SSIL and aperture. Similar to backside exposure method, UV exposure with mask#3 and backside exposure is performed after coating photoresist 10 μm-thickness. The parameters of photolithography are listed in Tab. 3.2. In comparison between the two self-alignment methods, the major difference is dose quantity of backside exposure. About surface tension modulation method, for want of dose quantity enough in backside exposure step, which is much smaller than that of backside exposure method, only the photoresist exposed with mask#3 and backside exposed in opening ring region will be removed after development. The remained photoresist is as the result illustrated in Fig. 3.1（e）. Besides, backside exposure method performs self-alignment in backside exposure step, whereas surface tension modulation method performs that in thermal reflowing step. Even though a little misalignment between the pedestal and the columnar photoresist is occurred in columnar photoresist defining step, the surface tension may drag the liquid-like photoresist to right position and correct the final shape of SSIL during heat treatment. Therefore, the integrated structure combined with SSIL and nano-aperture will be fabricated without misalignment（Fig. 3.1（g））.

Tab. 3.2 Basic parameters of coating AZ-4620 10 μm.

Process step	parameters	equipment
photoresist	AZ-4620	—
spin coating	1st Spin: 500 rpm for 10 sec 2nd Spin: 1200rpm for 40sec	JAPAN KYOWARIKEN K-359SD-1
Soft bake time	Baking at 90℃ for 90 sec	Hotplate
Exposure time	12 sec	JAPAN K-310P-100S
Development time	120-130 sec 【FHD-5】	—

Chapter 4 Results and measurements

4.1 Aperture

The designed parameters with different dimensions of aperture are discussed in chapter 2. The FIB patterning results is shown in Fig. 4.1（a） and （b）, where Au and Ti film in the defined area of aperture and opening ring is patterned and the Al layer exposes after ion bombardment. The diameter of pedestal is 15μm. It should be noted that a smaller dimensions of aperture is needed using a smaller ion current to pattern whereas the fabrication time will increase relatively. Fig. 4.2（a）～（e） show the fabrication results of apertures. The diameter of circular aperture is 103, 148, 329nm, respectively. The dimensions of C-shaped apertures are 303nm×205nm and 223nm×105nm which is also similar to the design parameters.

The opening ring has two functions, one is for fabricating the columnar photoresist without misalignment with the pedestal in backside exposure step and the other is for deciding diameter of SIL. Seeing that the aperture and opening ring are patterned by FIB in the same step, they are concentric. Following FIB patterning, the undercutting process is adopted to etch the sacrificial layer Al until the glass in the opening ring is exposed, as shown in Fig. 4.3.

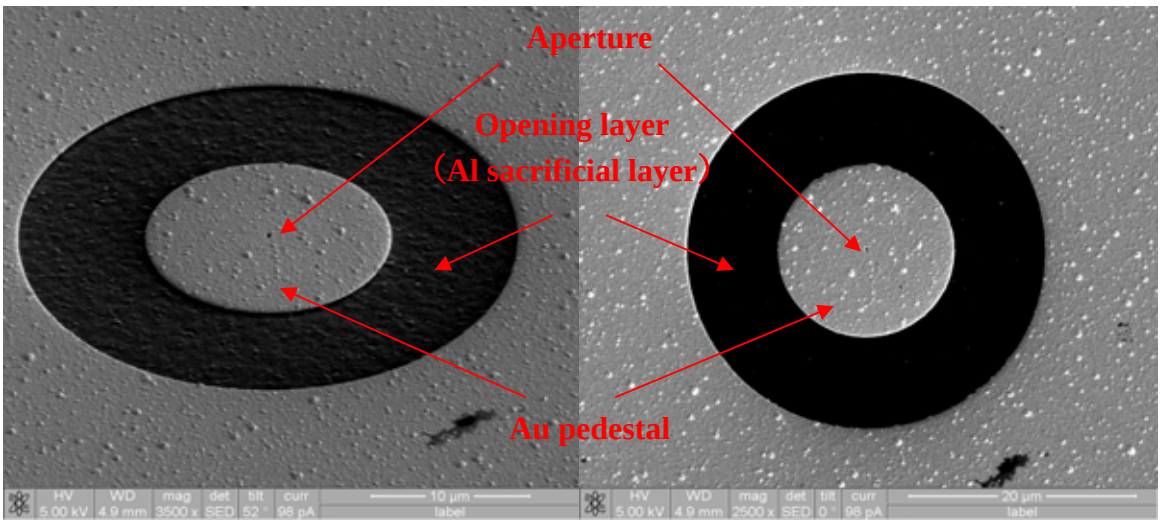

(a) (b)

Fig. 4.1 SEM image after FIB patterning.

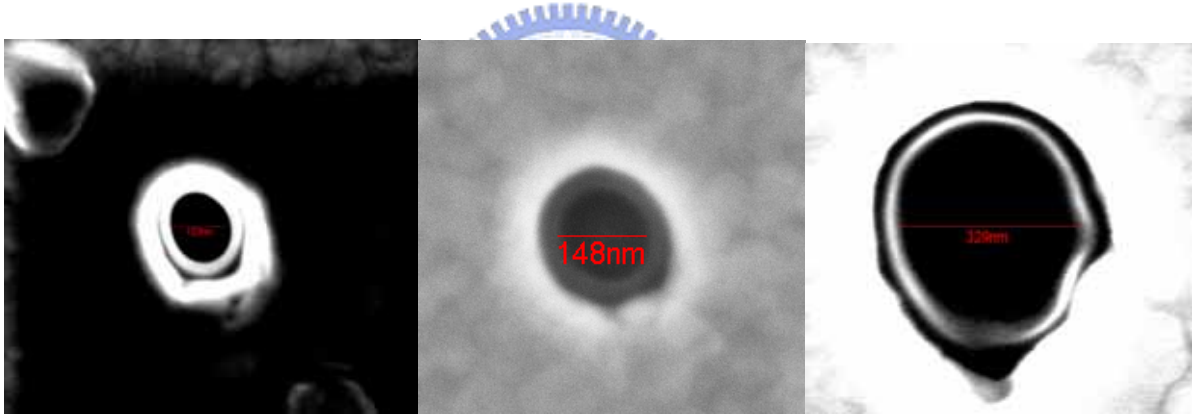

(a) φ103nm (b) φ148nm (c) φ329nm

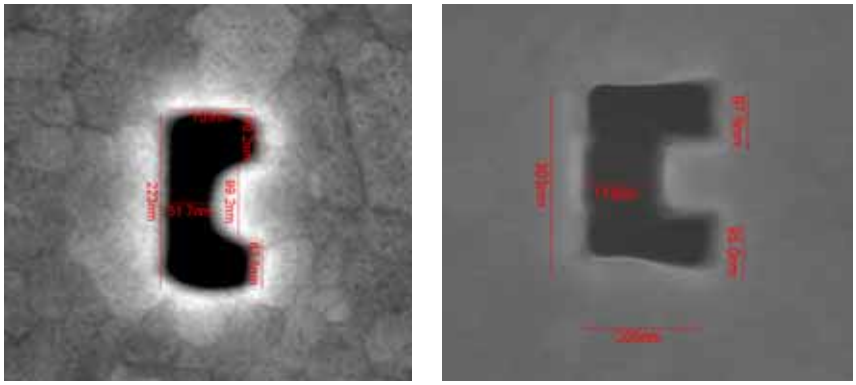

(d) 223nm×105nm (e) 303nm×205nm

Fig. 4.2 SEM images of the fabricated circular and C-shaped aperture with different dimensions.

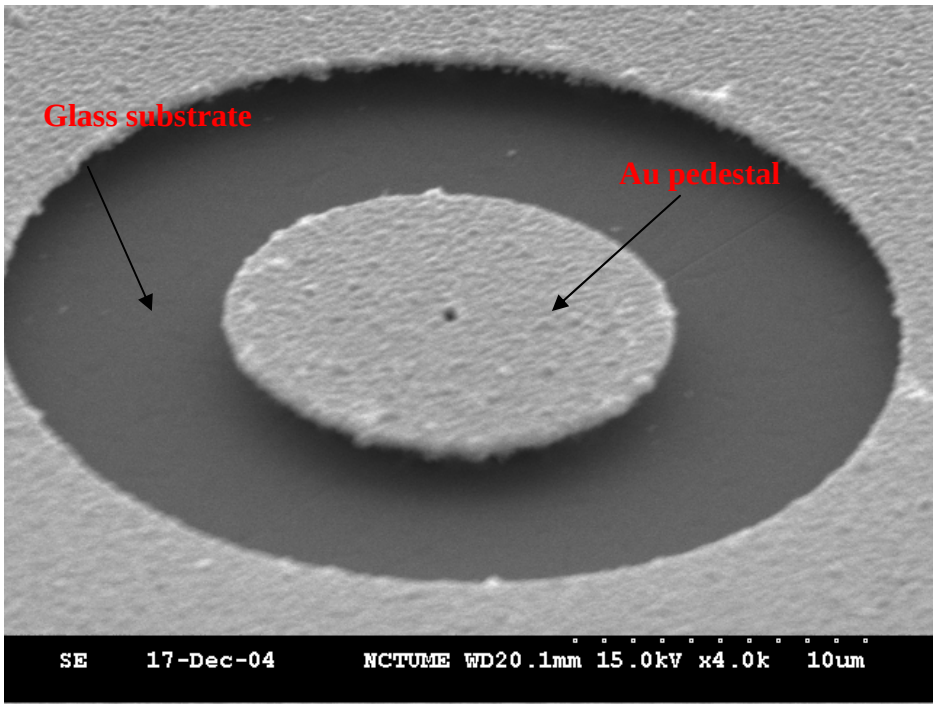

Fig. 4.3 SEM image after the undercutting process.

4.2 SIL

SIL with 15 μm-diameter are formed by the proposed method. Following performing UV exposure with mask#1 and backside exposure, the columnar photoresist on the pedestal layer is defined. Fig. 4.4（a） and （b） show the SEM images of columnar photoresist. Here, the Au pedestal is taken as mask in the backside exposure step.

From Fig. 4.4（b）, we can find that the columnar photoresist has some pattern loss of the diameter. This is seeing that UV light passing through the opening ring will result in light diffraction in backside exposure step, the photoresist on the edge of pedestal will be exposed and removed after development.

After photoresist patterning, the next process is heat treatment to form SIL in a 190℃ oven for 12hr. The SEM images of SIL combined with aperture are shown in Fig. 4.5（a）~（c）. Fig. 4.5（a）and（b）indicates that the SIL and aperture are integrated without misalignment, but there is a gap between the edge of pedestal and the edge of SIL which has existed after backside exposure. Even though the photoresist has experienced a heat

treatment at 190℃, the gap can not also be removed completely. This is the reason why the self-alignment process of backside exposure method has a difficulty fabricating SSIL but it can fabricate SIL combined with aperture easily. Fig. 4.5（c） shows the dimensions of SIL. The height and diameter of SIL is 7.77 μm and 14.92 μm, respectively.

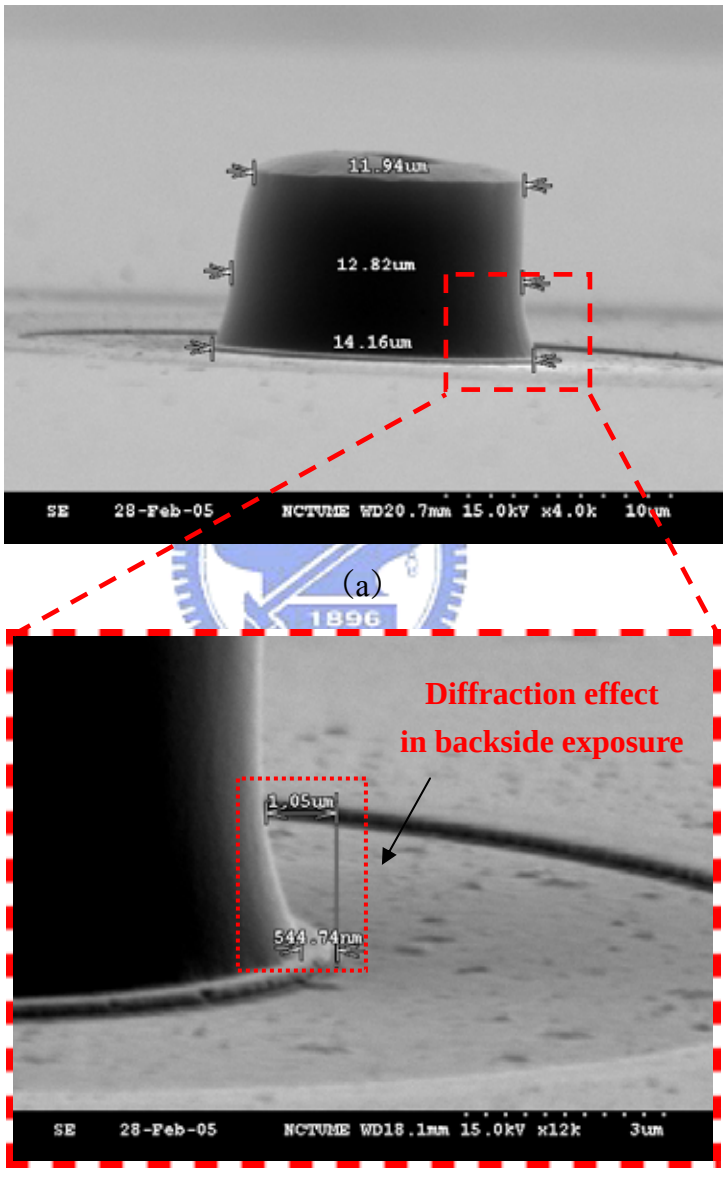

（a）

（b）

Fig. 4.4 SEM images of （a） the columnar photoresist after exposure with mask#1 and backside exposure and（b） showing the diffraction phenomenon in backside exposure step.

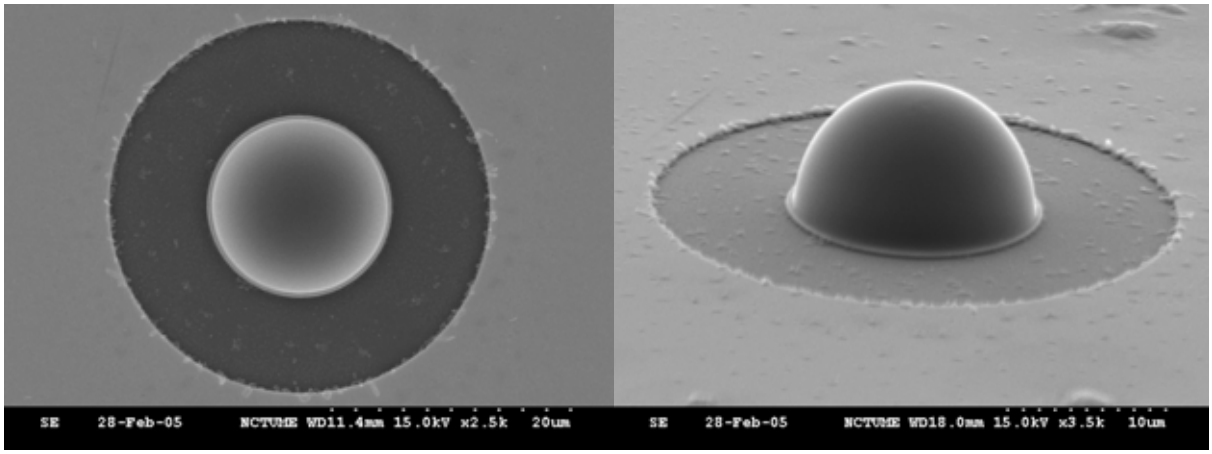

（a） （b）

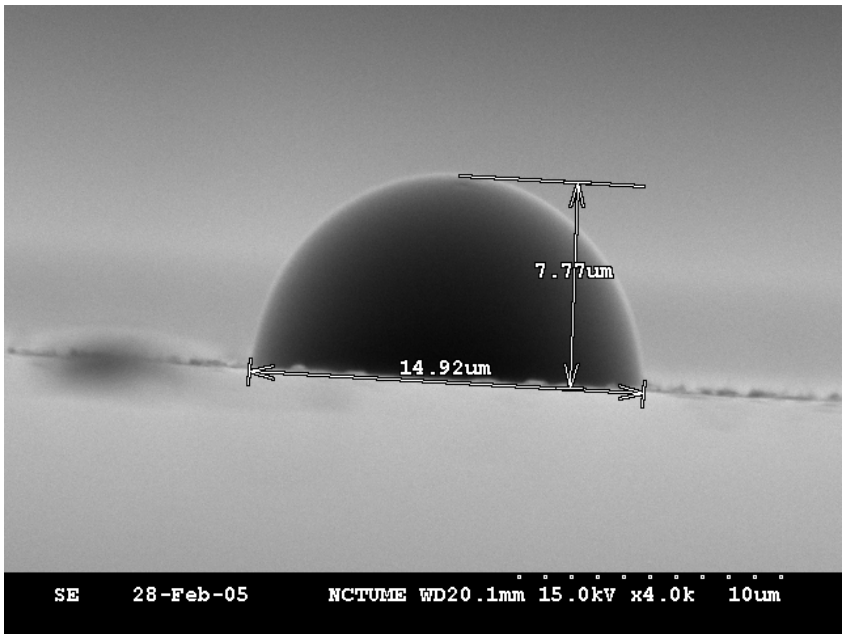

（c）

Fig. 4.5（a） and （b）SEM images showing the structure combined with SIL and aperture without misalignment.（c）Close-up SEM of SIL. SIL height =7.77 μm and diameter =14.92 μm.

4.3 SSIL

Here, the self-alignment process of surface tension modulation method is used to align SSIL and aperture precisely. Following performing UV exposure with mask#3 and backside exposure, the columnar photoresist on the pedestal layer is defined. Fig. 4.6(a)~(c) show the SEM images of columnar photoresist. Owing to lower exposure dose quantity which is not enough to expose the photoresist on the edge of pedestal in backside exposure step, there is no gap between the edge of columnar photoresist and the edge of pedestal after development. However, the misalignment between columnar photoresist and pedestal can not be avoided, as shown in Fig. 4.6(c), where the misalignment is 4.73 μm and the diameter of photoresist is about 25.08 μm.

After UV exposure and development, the columnar photoresist is also heated to form SSIL in oven at 190°C for 12hr, at which the liquid-like photoresist will tend to reduce itself surface energy and become a circular shape. Even though there is a little misalignment, the surface tension can drag the photoresist to right position and correct the final shape of SSIL. Therefore, the integrated structure combined with SSIL and nano-aperture is fabricated without misalignment, as shown in Fig. 4.7 (a) ~ (c). The diameter and radius of SSIL is about 17.82 μm and 9.00 μm, respectively. The height between the bottom and center of SSIL is 5.24 μm. Tab. 4.1 shows the comparisons between the designed parameters of SIL/SSIL and the fabrication results. The deviations are all less than 3%.

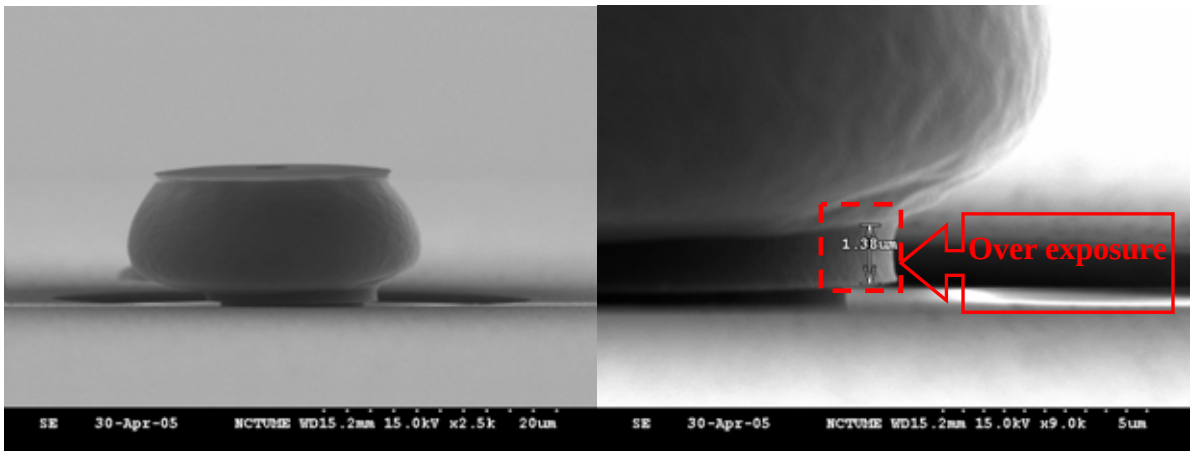

（a） （b）

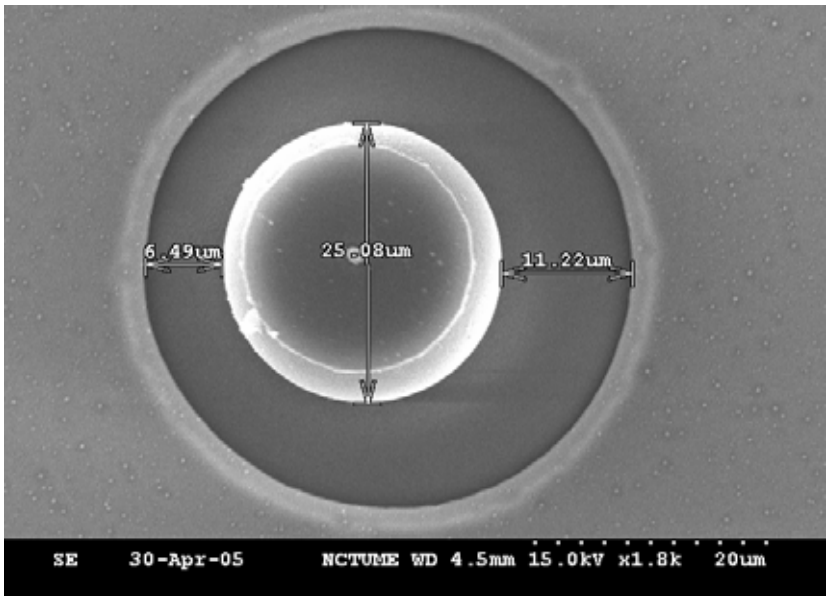

（c）

Fig. 4.6（a）SEM image after exposure with mask#3 and backside exposure. （b）Close-up SEM showing the over-exposure in backside exposure step. （c）SEM showing the misalignment = 4.73 μm between the pedestal and the columnar photoresist.

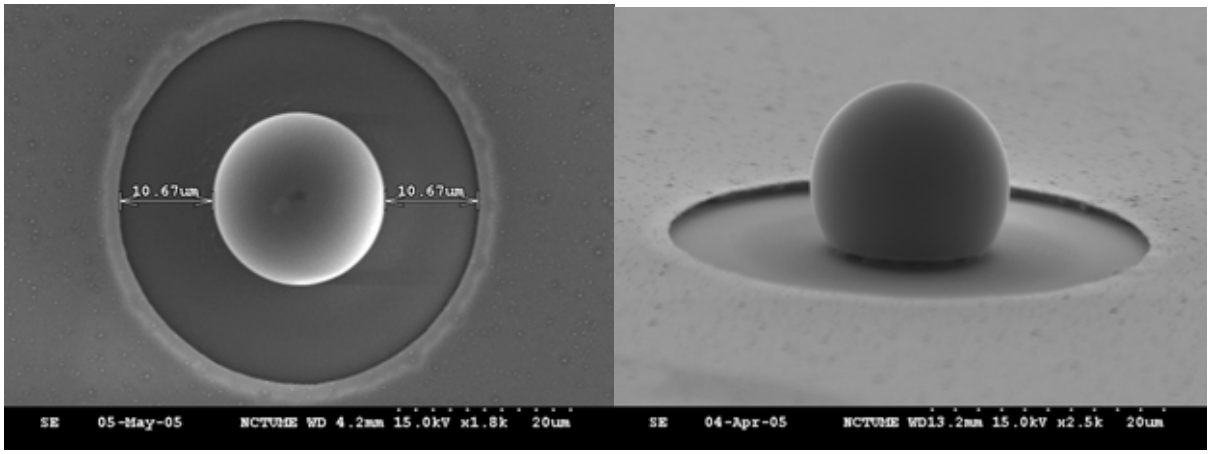

(a) (b)

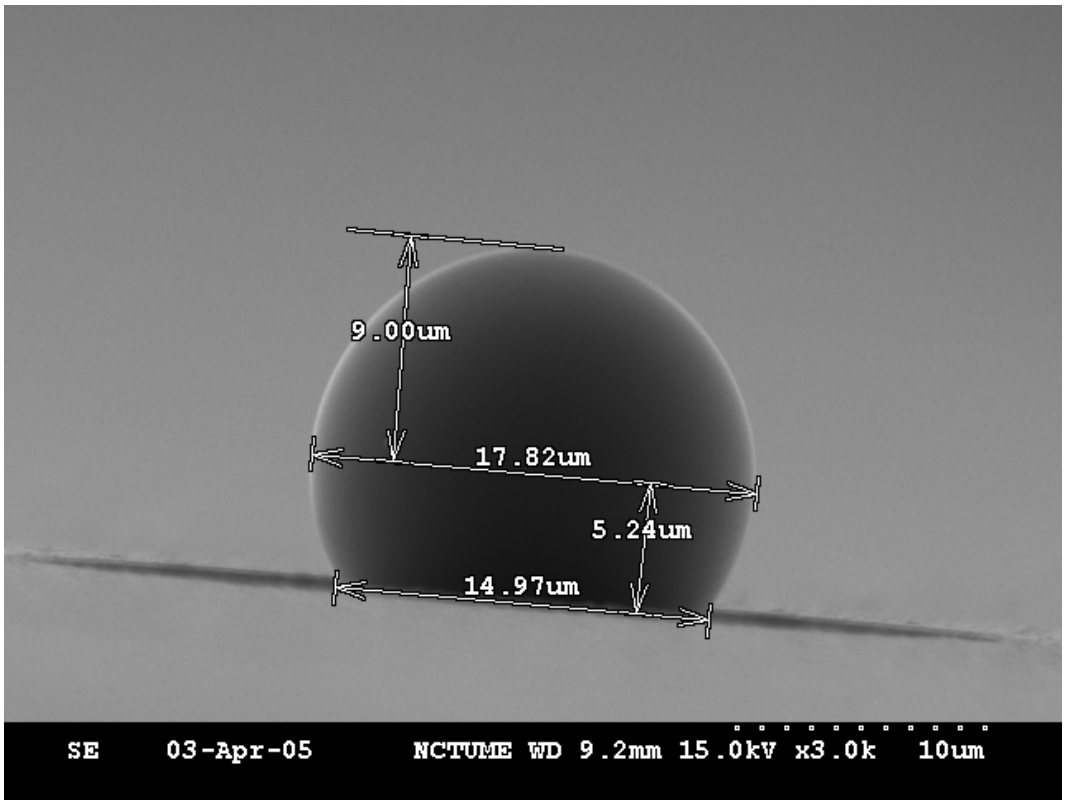

(c)

Fig. 4.7 (a) and (b) SEM images showing the structure combined with SSIL and aperture without misalignment. (c) Close-up SEM of SSIL. SSIL diameter =17.82 μm, radius =9.00 μm and height between the bottom and center of SSIL is 5.24 μm

Tab. 4.1 Comparison between designed parameters and fabrication results of SIL/SSIL.

SIL	Designed parameters (μm)		Fabrication results (μm)		deviation (%)	
	d	h	d’	h’	△ d	△h
ψ15	15	7.5	14.8	7.66	1.33	2.13
			14.9	7.70	0.67	2.67

SSIL	Designed parameters (μm)				Fabrication results (μm)				deviation (%)			
	d	r	b	h	d’	r’	b’	h’	△d	△r	△b	△h
ψ15	18.3	9.15	5.3	14.45	17.82	9.0	5.24	14.24	2.68	1.64	1.13	1.45
					17.94	8.9	5.20	14.1	1.97	2.73	1.89	2.42

d：The designed diameter of the SIL/SSIL

r：The designed radius of the SIL/SSIL

b：The designed distance between the bottom surface of SSIL and the center of the curved surface

h：The designed height of the SIL/SSIL

d’：The real diameter of the SIL/SSIL after reflowing thermally

r’：The real radius of the SIL/SSIL after reflowing thermally

b’：The real distance between the bottom surface of SSIL and the center of the curved surface

h’：The real height of the SIL/SSIL after thermal reflow

△d：（d- d’）/d

△r：（r- r’）/r

△b：（b- b’）/b

△h：（h- h’）/h

4.4 Far-Field measurement

It is restricted to available measurement equipment. In this section, the power throughput, spot size and reliability of SIL are measured with far-field experiment setup instead of near-field equipment.

As shown in Fig. 4.8, there are four cases to be measured, including spot size calibration of fiberlens, spot size and power throughput calibration of SIL, spot size and power throughput calibration of aperture, and spot size and power throughput calibration of SIL/aperture component. The kinds of apertures include circular apertures and C-shaped apertures.

In this scheme, light is guided by the core of a single-mode fiber and focused on the sample by the front-end fiber-lens. After light passing through the sample, the diverging or diffracting light will be collected and collimated by objective lens of which the focal plane should be adjusted to the focal spot of the incident light so that the output light through objective lens will be collimated. Finally, the output beam size is detected by CCD camera. Owing to output beam collimated by objective lens, CCD camera at different position will detect the same beam size which is defined as full-width at 1/e2 maximum intensity. This method results in the output beam larger than diffraction limit and need not precisely control the position of the objective lens and CCD camera.

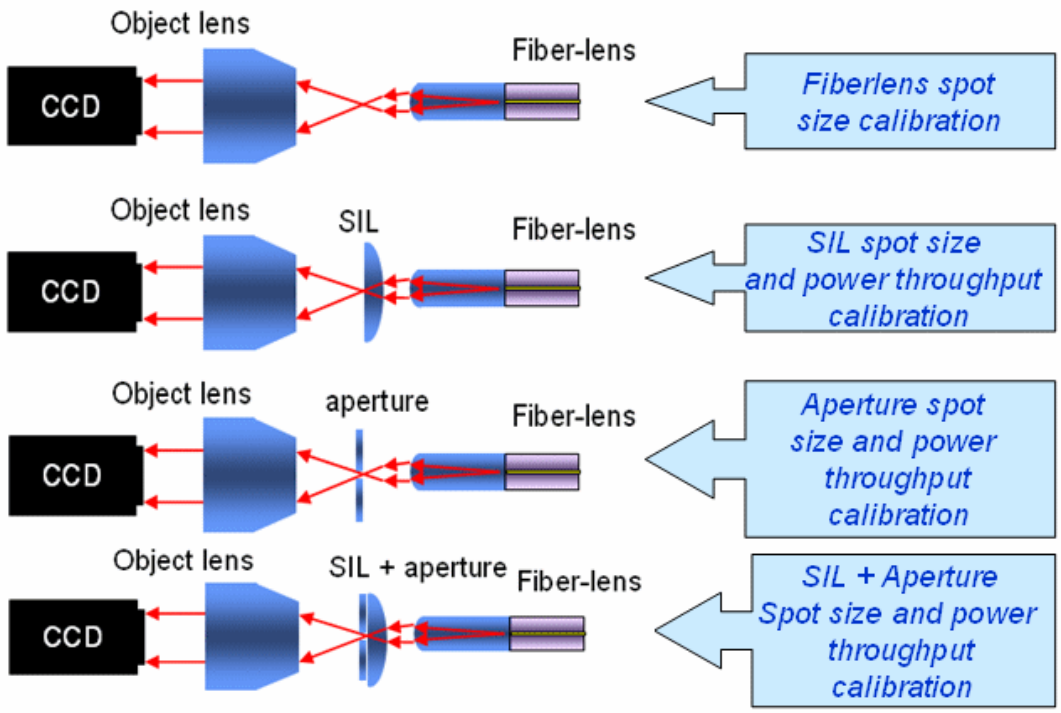

Fig. 4.8 Schematic diagrams of four cases for measurement.

4.4.1Principle

By CCD capturing, what we really measured is not the focused spot size but the collimated output beam size; therefore, we use the Gaussian beam condition to calculate spot size according to fundamentals of photonics.

If a lens is placed at the waist of a Gaussian beam, as shown in Fig. 4.9, the transmitted beam is then focused to a waist radius W_0' at a distance z' given by :

$$W_0^{'} = \frac{W_0}{\left[1-(Z_0/f)^2\right]^{1/2}} \quad \text{.....4-1}$$

$$z^{'} = \frac{f}{1+(f/z_0)^2} \quad \text{.....4-2}$$

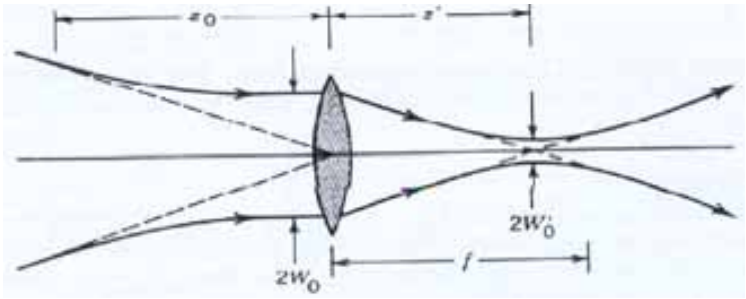

Fig. 4.9 Focusing a beam with a lens at the beam waist.

If the depth of focus of the incident beam $2z_0$ is much longer than the focal length f of the lens, as shown in Fig. 4.10, Eq. 4-1 and Eq. 4-2 can be simplified as：

$$W_0^{'} = \left(\frac{f}{z_0}\right) W_0 \quad \text{..... 4-3}$$

$$z^{'} = f \quad \text{.....4-4}$$

z_0 is defined as $\pi W_0^2 / \lambda$. Therefore, Eq. 4-3 can be further expressed as follows：

$$W_0^{'} = \frac{\lambda}{\pi W_0} f = \theta_0 f \quad \text{.....4-5}$$

In wave optics, the focused waist radius W0' is directly proportional to the wavelength and the focal length, and inversely proportional to the radius of the incident beam. The spot size $2W_0^{'}$ focused by objective lens can be derived as follows：

$$2W_0^{'} = \frac{4}{\pi} \lambda \frac{f}{2W_0} \quad \text{.....4-6}$$

Where $2W_0$ can be defined as the beam size collimated by objective lens in our measurement setup.

It should be noted that as light passes through a nano-aperture, the spot size is determined by dimensions of aperture. Nevertheless, the light through a nano-aperture will result in light diffraction. It is clear that the larger light diffraction is occurred at the same aperture size, the larger output beam size is detected by CCD. Therefore, Eq.4-6 can be applied to obtain the spot size focused by fiberlens or by fiberlens and SIL while can not be

applied to obtain the spot size of nano-aperture owing to light diffraction effect not resembling principle of focus.

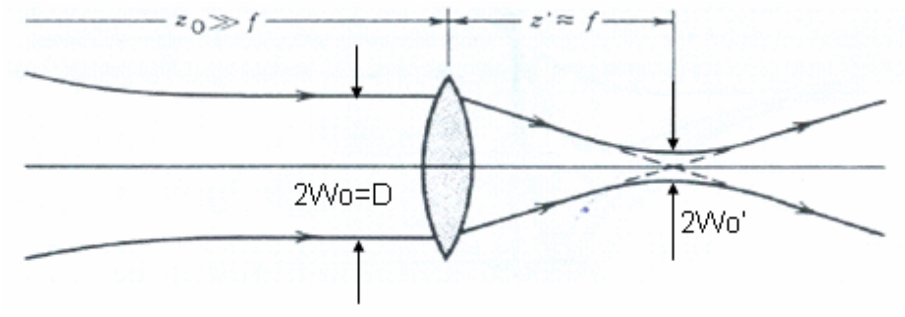

Fig. 4.10 Focusing a collimated beam.

4.4.2 Experiment setup

In this research, the far-field measurement system is shown in Fig. 4.11. The equipments include 633nm laser diode for providing light source, fiberlens with 460μm length for focusing laser beam, objective lens with 10×N.A.0.4 for collimating output beam, CCD for detect the collimated output beam, sensor for detecting light power, power meter for measuring power light and optical microscope（OM）for observing the position of light spot focused by fiberlens on the sample. During spot size measurement, 633nm laser beam is coupled and guided into the optical fiber and then focused by the front-end fiber-lens whose focal length is about 200μm. After light passing through the target（SIL, aperture or SIL/aperture component）on sample, the output beam is collected and collimated by objective lens whose focal length is about 1.6cm. Finally, the collimated beam size is detected by CCD. Fig. 4.12 shows the condition of fiberlens focusing laser on the sample. In order to confirm the components（fiberlens, target on sample, objective lens and CCD camera） in alignment, the fiberlens, objective lens and sample are all set a 3-axial position stage to control the relative positions. Tab. 4.2 lists the specification of CCD camera.

Following capturing the spot image by capture card without compression, the intensity profile of output beam is gotten by using Matlab to write the program. Since the ambient

light is an influence on these measurements, its power is measured to be compared with the power of transmitted spot. As the spot size focused by fiberlens wants to be measured, the sample held by 3-axial position stage must be removed.

About measuring power throughput, the power sensor will be set at the back of objective lens to detect light power and then detected signal will be transfer to power meter.

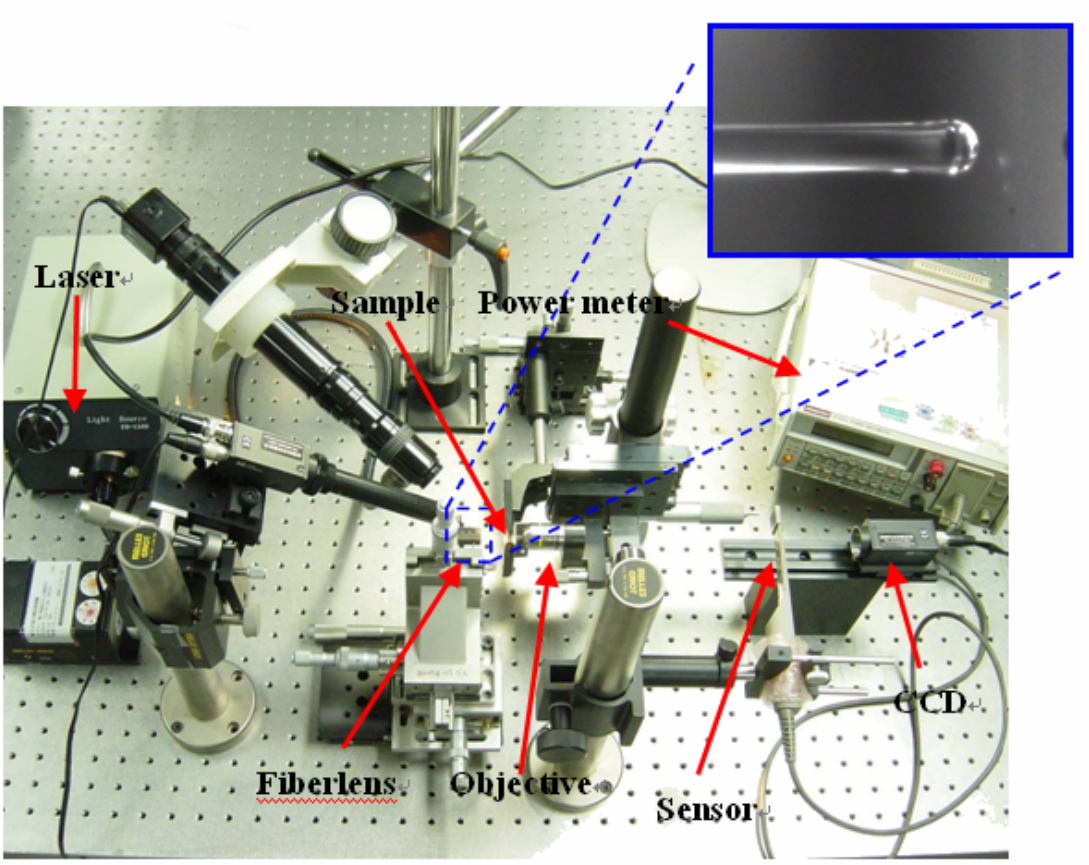

Fig. 4.11 Illustration of the far-field measurement system.

Fig. 4.12 The condition of fiberlens focusing laser on the sample.

Tab. 4.2 Specification of CCD camera.

Pick-up device	1/3 type CCD
Effective picture elements	659(H) X 497(V)
Sensing area	7.4μm X 7.4μm
Horizontal frequency	15.734 kHz
Vertical frequency	59.94 Hz

4.4.3Measurement results

In spot size calibration, the first measurement result is for comparing whether SIL can focus the incident light and reduce the spot size focusing on the bottom of SIL or not. After the spot size focused by fiberlens is collimated by objective lens, the spot of collimated beam is captured by CCD camera, as shown in Fig. 4.13（a）. Then, the intensity profile of collimated beam is calculated by using Matlab software and shown in Fig. 4.13（b）. According to Fig. 4.13（b）and Eq. 4-6, the spot size focused by fiberlens is about 5.44μm.

Here, the spot size focused by fiberlens and 15μm diameter SIL is also measured by far-field measurement system. Fig. 4.14 shows the spot detected by CCD camera which is formed by several CCD images because the CCD camera can not capture the complete spot. Consequently, the profile of collimated beam can not be obtained by using Matlab software. Compared with the beam size in Fig. 4.13（a）, the beam size in Fig. 4.14 is larger. This means that the SIL can really focus the incident light and shrink the spot size on the bottom of

SIL.

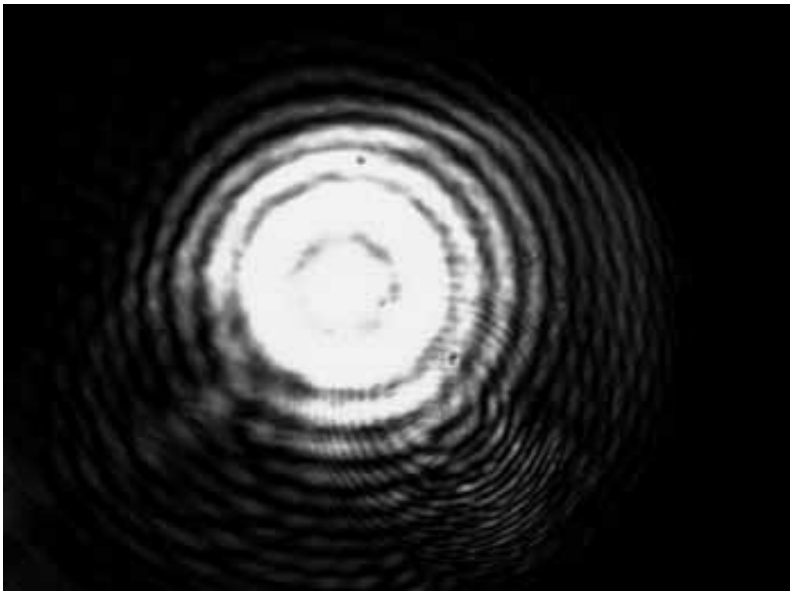

（a）

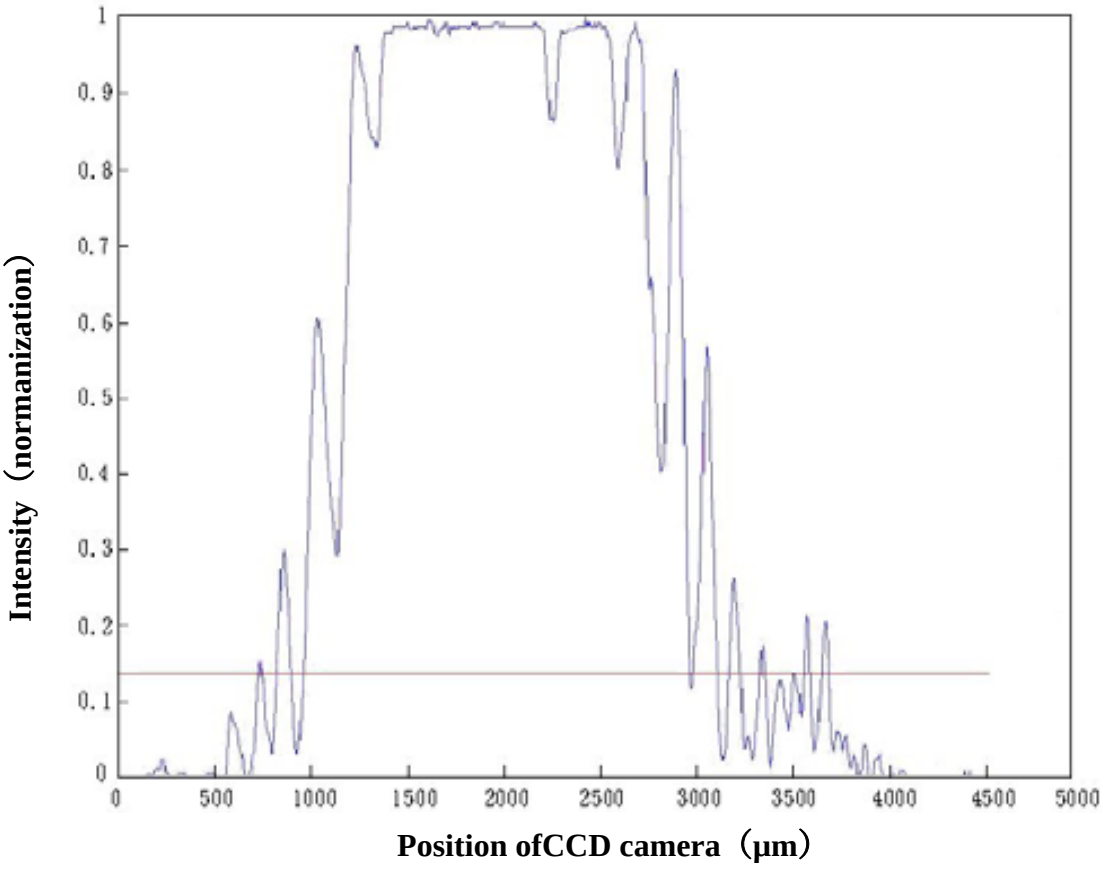

（b）

Fig. 4.13（a）showing the collimated spot without SIL captured by CCD camera.（b）showing the intensity profile obtained by Matlab software. The spot size is 5.44μm.

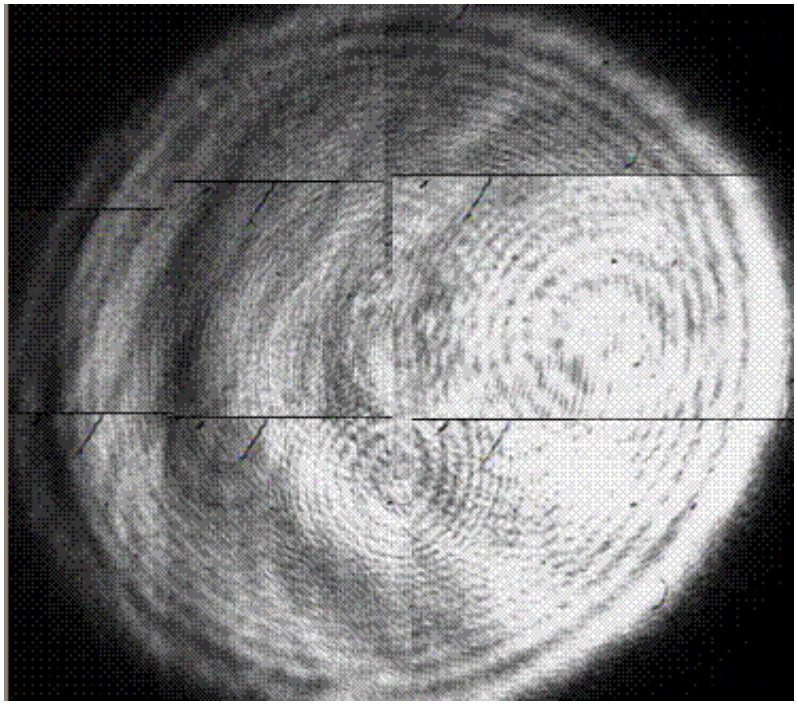

Fig. 4.14 The collimated spot with 15μm diameter SIL captured by CCD camera.

After verifying SIL can reduce the focused spot size on the bottom of SIL, the nano-aperture integrated with 15μm diameter SIL is also measured whether SIL can improve light throughput with good resolution or not. At first, the sample of only aperture and 15μm diameter SIL/aperture components is set to the far-field measurement system, respectively. Following CCD camera capturing the spot image, the beam profile is also obtained by Matlab software.

Fig. 4.15 shows the intensity profile focused by fiberlens with 313nm diameter circular aperture. Fig. 4.16 shows the intensity profile focused by fiberlens and 15μm diameter SIL with 313nm diameter circular aperture. Eq.4-1 can not be applied to obtain the spot size of nano-aperture because the spot size through nana-aperture is determined by dimension of aperture and light diffraction effect does not resemble principle of focus, as described in above section. It is noticeable that since the recording disk and near-field peak up head has a

air gap（or flying height）which will result in light diffraction effect during data storage, the spot size illuminating disk will be larger than that passing through aperture. It is apparent that the beam size in Fig. 4.16 is smaller than in Fig. 4.15. This can at least indicate that the aperture/SIL component can lower the light diffraction because laser beam in SIL can shrink its wavelength so that the performance of near-field pick up head integrated with SIL and aperture can be improved. Moreover, the aperture/SIL component can also smooth the beam profile.

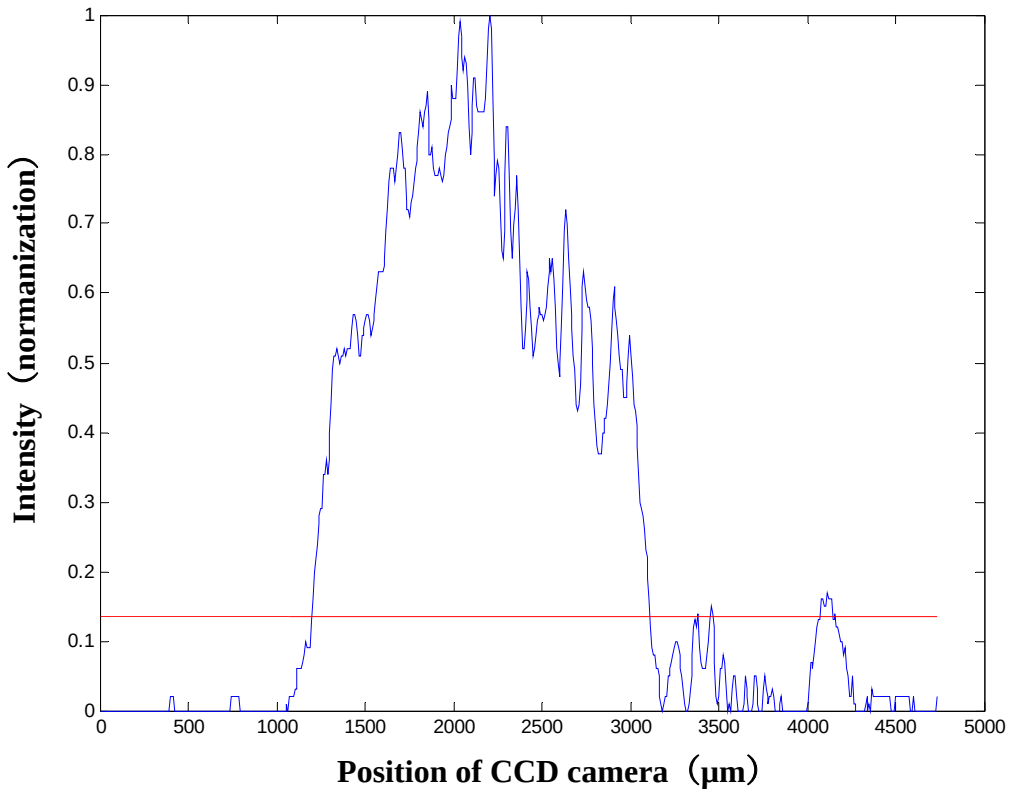

Fig. 4.15 The intensity profile focused by fiberlens with diameter 313nm of aperture.

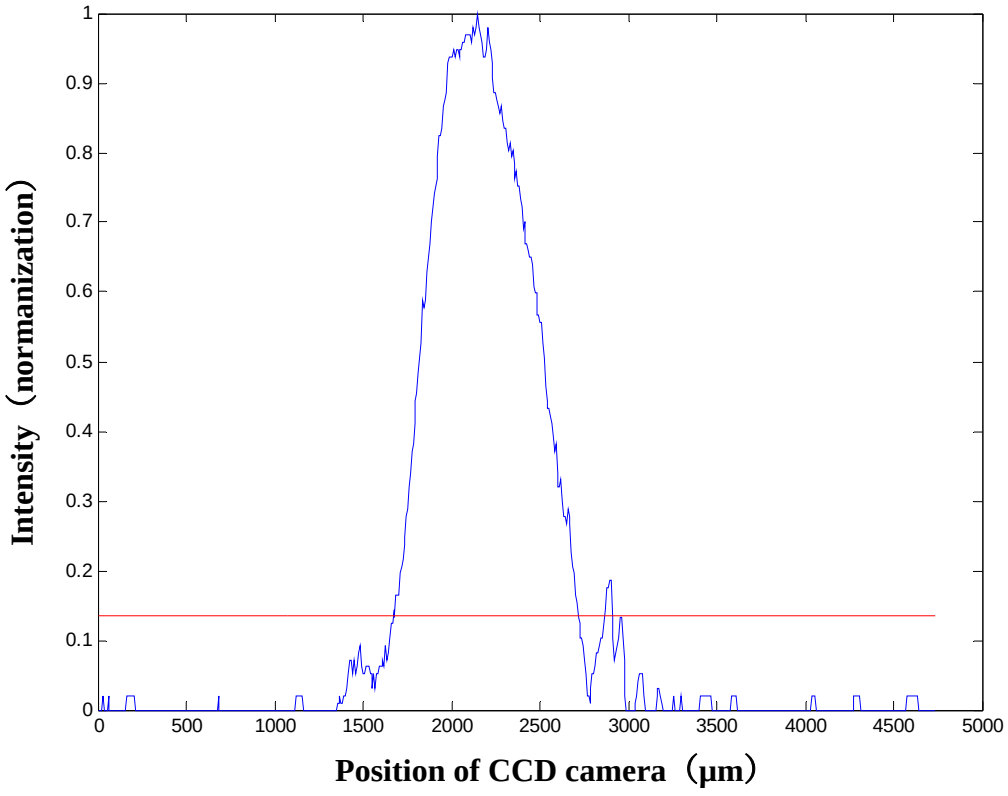

Fig. 4.16 The intensity profile focused by fiberlens and diameter 15μm of SIL with diameter 313nm of aperture.

After spot size calibration, the light transmission is then measured by power meter. At first the power sensor is set to between CCD camera and objective lens. When collimated laser beam passes through the sensor, the power meter will detect the light power. In order to minimize the errors of measurement, the all of sample are measured with 3 cycles and the 3 measured results of each sample are averaged. Tab. 4.3 shows the measurement results of transmission and throughput and then Tab. 4.4 shows the comparisons between enhancement factors. Here, we use throughput to test the transmission performance, where hroughput is defined as the ratio of the total transmitted power through the aperture to the total incident power over the aperture area. Seeing that ambient noise（5nW） is relatively very small compared to incident laser power, the measured results are believable.

About transmission measurement of 15μm diameter SIL, the input power is about 0.914μW and then the measured output power is about 0.596μW. Therefore, the transmission of diameter 15μm of SIL is about 65.2%. This observed data resembles the predicted data. The far-field measurement results show that the smaller diameter of circular aperture is measured, the smaller light throughput is obtained. It is clear that 329nm-diameter circular aperture/15μm-diameter SIL component can really enhance the light throughput by a factor of 1.620 in comparison with 329nm-diameter circular aperture alone. This result shows that SIL can really enhance the light power through the aperture and the feasibility of self-alignment technique between SIL and nano-aperture is further verified. Nevertheless, the light throughput of 148nm-diameter circular aperture/15μm-diameter SIL component is just 1.142 times larger than 150nm-diameter circular aperture alone. This phenomenon seems likely that as aperture size is about 148nm, the throughput is almost determined by aperture and most light is prevented from passing through the aperture. For this reason, SIL can not enhance the throughput obviously.

In addition to circular aperture, C-shaped aperture is also measured. Theoretically, C-shaped aperture, which can be viewed as a ridge waveguide, can overcome the large attenuation due to cross-sectional area and exhibits waveguiding properties so the light throughput should be enhanced greatly. In the measurement results, compared with 148nm-diameter circular aperture, the throughput of 303nm×205nm C-shaped aperture is about 14.325 times enhancement, while maintaining a comparable near-field spot size. It is noticeable that the dimensions of aperture determine transmission mode. This is the reason why the throughput of 223nm×105nm C-shaped aperture is 4.895 times larger than that of 303nm×205nm C-shaped aperture. Although this measurement result matches the trend of simulation result, the enhancement effect is not as good as the simulation result. This phenomenon may be that since the equipment setup is a far-field system, the enhancement effect of near-field can not be observed by measurement result. The rounding and tapering

inherent in FIB milling is also the reason that the throughput enhancement of measurement result is less than that of simulation result. In addition, since SIL can enhance the side incident light illuminating C-shaped aperture, the throughput of 303nm×205nm C-shaped aperture/15μm-diameter SIL component can be greatly enhanced by 1.706 times as compared with 303nm×205nm C-shaped aperture alone, even can enhanced by 24.438 times as compared with 148nm-diameter circular aperture alone. This measurement result indicates that combination of SIL and C-shaped aperture can really greatly enhance the performance of near-field pick-up head.

Tab. 4.3 The measurement results of transmission and throughput.

Sample	Spot area (μm^2)	Transmission	Throughput
Only fiberlens	23.24	100%	—
Only SIL	9.03	65.2%	0.072
Circular aperture (d=329nm)	0.0850	1.838%	0.216
Circular aperture (d=148nm)	0.0172	0.028%	0.0163
Circular aperture (d=103nm)	0.0079	0.009%	0.0093
SIL + Circular aperture (d=329nm)	0.0850	2.955%	0.350
SIL + Circular aperture (d=148nm)	0.0172	0.032%	0.0186
C-shaped aperture (303nm〤205nm)	0.05	1.167%	0.2335
C-shaped aperture (223nm〤105nm)	0.0201	2.240%	1.1143
SIL+C-shaped aperture (303nm〤205nm)	0.05	1.991%	0.3983

- **Transmission：Output power / Input power**
- **Throughput：Transmission / Spot area**

Tab. 4.4 The comparisons between the throughput enhancements.

Target sample	Compared sample	Enhancement
SIL + Circular aperture (d=329nm)	Circular aperture (d=329nm)	1.620×
SIL + Circular aperture (d=148nm)	Circular aperture (d=148nm)	1.142×
C-shaped aperture (303nm×205nm)	Circular aperture (d=329nm)	14.325×
	Circular aperture (d=148nm)	1.081×
C-shaped aperture (223nm×105nm)	Circular aperture (d=329nm)	68.36×
	Circular aperture (d=148nm)	5.159×
	C-shaped aperture (303nm×205nm)	4.895×
SIL+C-shaped aperture (303nm×205nm)	C-shaped aperture (303nm×205nm)	1.706×
	Circular aperture (d=148nm)	24.438×

- **Enhancement：Target sample / Compared sample**

4.4.4 SIL/SSIL reliability

The duration test of SIL is also measured. The incident light power is about 0.328mW. After laser destruction for 12hr, the SEM image of SIL is shown in Fig. 4.17. Compared with SIL without laser destruction, the profile of SIL with laser destruction does not change.

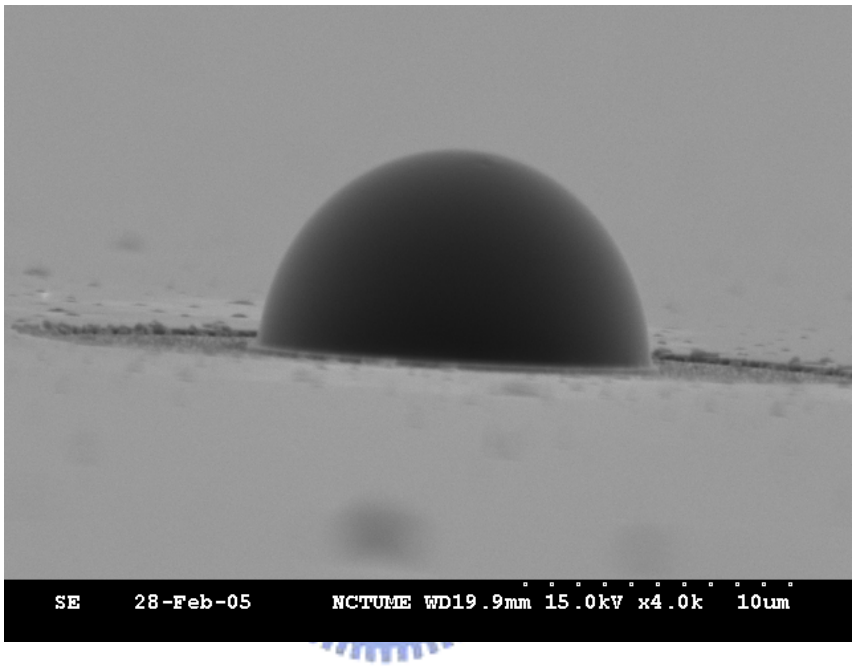

Fig. 4.17 SEM image of SIL after 0.328mW of laser power destruction for 12hr.

4.5 Properties of AZ-4620 with different reflowing time

The refractive index（n）and absorption coefficient（k）measured by spectroscopic ellipsometry are plotted as Fig. 4.18（a）and（b） as a function of wavelength for the AZ-4620 films reflowed at 190℃ with different reflowing time. It is found that increasing reflowing time can improve the refractive index but lower the absorption coefficient, which is particularly apparent at ultraviolet（UV）wavelength. This is believed that increasing reflowing time will vaporize the residual solvent further in AZ-4620 film and increase the density of AZ-4620. The refractive index almost does not change with the reflowing time

over 6 hr. The higher absorption coefficient means the lower transparency of AZ-4620 film relatively, which results in the lower light transmission efficiency through the same thickness of film.

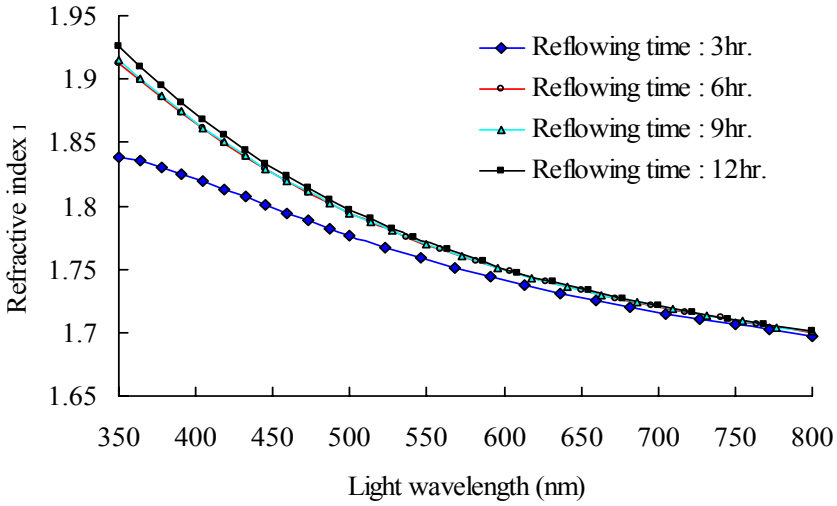

(a)

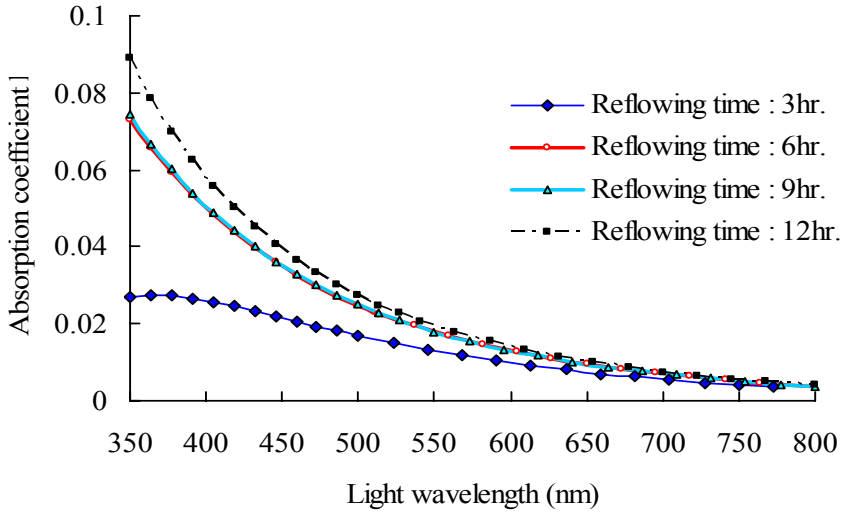

(b)

Fig. 4.18 (a) The refractive index for AZ-4620 films reflowed at 190℃ with different reflowing time. (b) The absorption coefficient for AZ-4620 films reflowed at 190℃ with different reflowing time.

Chapter 5 Summary

5.1 Conclusion

A near-field pick-up head combined with nano-aperture and SIL/SSIL is achieved by MEMS technology. The self-alignment technique is adopted to overcome the misalignment between the SIL/SSIL and aperture component. By combining SIL/SSIL and aperture together, a small spot size with good light throughput can be obtained.

By SEM measurements, the maximum error of fabricated SIL/SSIL is less than 3% in comparison with the designed values. About aperture design, the diameter 103nm, 148nm, and 329nm of circular apertures and the dimensions 303nm×205nm and 223nm×105nm of C-shaped apertures are fabricated by FIB.

From the measurement results by the far-field equipment setup, the transmission of 15μm-diameter SIL is about 65.2% as well as SIL is verified to can really focus the incident light and reduce the spot size on the bottom of SIL. The 329nm-diameter aperture combined with 15um-diameter SIL can show 1.62 times enhancement of the light throughput in comparison with 329nm-diameter aperture alone. It is also found that since light in the SIL/SSIL can reduce its wavelength by a factor of n for SIL or n^2 for SSIL, it passing through the aperture can decrease the light diffraction. Therefore, the performance of near-field pick up head integrated with SIL and aperture can be improved. Moreover, the aperture/SIL component can also smooth beam profile.

About measurement results of C-shaped aperture, the throughput of 300nm×200nm C-shaped aperture is about 1.081 times enhancement as compared with 329nm-diameter circular aperture , even can enhance the throughput by 14.325 times as compared with 148nm-diameter circular aperture. In comparison between C-shaped apertures, the

throughput of 223nm×105nm C-shaped aperture is 4.895 times larger than that of 303nm×205nm C-shaped aperture. This result matches the trend of simulation result but the enhancement effect is not as good as the simulation result. Then, the 303nm×205nm C-shaped aperture/15um-diameter SIL component also shows a 1.706 times enhancement of throughput as compared with 303nm×205nm C-shaped aperture alone, even shows a 24.438 times enhancement of throughput as compared with 148nm-diameter circular aperture alone. About duration test, the profile of SIL is not damaged after 0.328mW of laser power destruction for 12hr.

5.2 Discussion

It is restricted to available measurement equipment. The far-field measurement system is used instead of near-field measurement system. Nevertheless, the spot size calibration of nano-aperture and enhancement effect of near-field can not be observed by far-field system. For this reason, we also try to use Near-Field Scanning optical microscope （NSOM）to verify our researches in the future.

References

1. C. Mihalcea, W. Scholz, S. Werner, S. Wunster, E. Oesterschulze, and R. Kassing "Multipurpose sensor tips for scanning near-field microscopy" Appl. Phys. Lett., Vol. 68, 1996.

2. Chung-Hao Tien, Yin-Chieh Lai, Tom D. Milster, and Han-Ping Shieh "Design and Fabrication of Fiberlenses for Optical Recording Application", ISOM, pp.230-231, 2001.

3. Daniel A. Fletcher, Dmitrii Simanovskii, Daniel Palanker, Kenneth B. Crozier, Calvin F. Quate, S Kino. Gorden, and Kenneth. E Goodson "Microfabricated Solid Immersion Lens with Metal Aperture."IEEE , pp.133-134, 2000.

4. Gordon R. Knight, TeraStor Corporation, and San Jose, "Near-Field Recording" http://www.nswc.navy.mil/cosip/nov98/sugg1198-2.shtml.

5. Jong Uk Bu, Youngjoo Yee, See-Hyung Lee, and Jinhong Kim "MEMS Technology for Optical Data Storage" Transducer, pp. 1762-1767, 2003.

6. Jen-Yu Fang, Wan-Ting Lin, Chung-Hao Tien1, Yi Chiu2 and Han-Ping D. Shieh "C-shaped aperture for near-field recording" ISOM, 2004

7. J. A. Matteo, D. P. Fromm, Y. Yuen, P. J. Schuck, W. E. Moerner, and L. Hesselink "Spectral analysis of strongly enhanced visible light transmission through single C-shaped nanoapertures" Appl. Phys. Lett., 2004.

8. Kenneth B. Crozier, Daniel A. Fletcher, Gordon S. Kino, and Calvin F. Quate, "Micromachined Silicon Nitride Solid Immersion Lens" JOURNAL OF MEMS, Vol. 11, NO. 5, OCTOBER 2002

9. Kenji Kato, Usumu Ichihara, Nobuyuki Kasama, Manabu Oumi, Takashi Niwa, Yasuyuki Mitsuoka, and Kunio Nakajima "Small-sized Near-Field Optical Head Structure With high throughput"

10. Meng-Yu Wu, Yi Chiu, Han-Ping Shieh, Wensyang Hsu, and Hsueh-Liang Chou "Fabrication of planar integrated optical pick-up heads" 2003.

11. PHAN Ngoc Minh, Takahito ONO, and Masayoshi ESASHI, “A novel fabrication method of the tiny aperture tip on silicon cantilever for near field scanning optical microscopy,” Micro Electro Mechanical Systems, 1999. Twelfth IEEE International Conference on 1999, pp. 360-365.

12. Saeed Pilevar, Klaus Edinger, Walid Atia, Igor Smolynianov, and Christopher Davis “Focused ion-beam fabrication of fiber probes with well-defined apertures for use in near-field scanning optical microscopy” Appl. Phys. Lett., Vol. 72, 1998.

13. Trans Lane, and Wensyang Hsu, “Fabrication of Sub-micron Optical Apertures by An Over-electroplating Method”, ISOM, pp. 252-253, 2001.

14. Tom D. Milster, Farhad Akhavan, Melissa Bailey, J. Kelvin Erwin, David M. Fellx, Kusato Hirota, Steven Koester, Kei Shimura and Yan Zhang “Super-Resolution by Combination of a Solid Immersion Lens and an aperture” Jpn. J. Appl. Phy. Vol. 40, pp. 1778-1782, 2001.

15. Xiaolei Shi and Lambertus Hesselink “Mechanisms for Enhancing Power Throughput from Planar Nano-Apertures for Near-Field Optical Data Storage” Jpn. J. Appl. Phys., 2002.

16. Xiaolei Shi, Lambertus Hesselink and Robert L. Thornton “Ultrahigh light transmission through a C-shaped nanoaperture” OPTICS LETTERS, 2003.

17. Yoshimasa Suzuki, Hiroshi Fuji, Junji Tominaga, Takashi Nakano, and Nobufumi Atoda “Near-field aperture fabricated by solid–solid diffusion” Vol. 77, No 234, December 2000.

18. Youngjoo Yee, Jong Uk Bu, Il-Joo Cho, Euisik Yoon, Su-Dong Moon, and Shinill King “ Micro Solid Immersion Lens Fabricated By Micro-molding For Near-Field Optical Data Storage” IEEE, 2000.

19. Yuh-Sheng Lin, Cheng-Tang Pan, Kun-Lung Lin, Shih-Chou Chen, Jauh-Jung Yang, and Jei-Pin Yang “Polyimide as the pedestal of batch fabricated micro-ball lens and micro-mushroom array” IEEE, 2000.

20. Yu-Ru Chang, Yi Chiu, and Wensyang Hsu “Development of self-alignment process between SIL/SSIL and aperture for Near-Field Recording Pick-up Head” APDSC, pp. 208-209, 2004

21. 周學良,徐文祥“結合光纖插孔、固態浸沒式透鏡與精密電鍍微孔之光學讀取頭”國立交通大學機械工程研究所 91 年 7 月

22. 周協利, 魏培坤“近場光學光譜儀於次微米狹縫之研究”國立海洋大學/光電科學研究所 89 年 7 月

23. 吳孟諭, 謝漢萍“應用在近場光學記錄的光纖讀寫頭模組”國立交通大學光電工程所 91 年 7 月

24. 林盈熙,“奈米級之資料儲存技術,”第二屆奈米工程既系統技術研討會, pp.2-31~2-39, 1999

25. 蔡定平,“近場光碟機最近的發展,”科儀新知, Vol. 19, No. 4, pp.28-37, February 1998